Experimental Neurology 385 (2025) 115128

Contents lists available at ScienceDirect

Experimental Neurology

journal homepage: www.elsevier.com/locate/yexnr

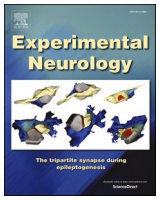

Research paper

Effects of ALS-associated 5'tiRNA$^{Gly\text{-}GCC}$ on the transcriptomic and proteomic profile of primary neurons in vitro

Elisabeth Jirström [a,b], Anna Matveeva [a,b], Sharada Baindoor [a], Paul Donovan [a,b], Qilian Ma [a,b,c], Elena Perez Morrissey [a,b], Ingrid Arijs [d,e], Bram Boeckx [d,e], Diether Lambrechts [d,e], Amaya Garcia-Munoz [f], Eugène T. Dillon [g], Kieran Wynne [f], Zheng Ying [c], David Matallanas [f], Marion C. Hogg [a,b,1], Jochen H.M. Prehn [a,b,*]

[a] Department of Physiology and Medical Physics, Royal College of Surgeons in Ireland, 123 St. Stephen's Green, Dublin 2, Ireland
[b] FutureNeuro Research Ireland Centre, Royal College of Surgeons in Ireland, Dublin 2, Ireland
[c] Jiangsu Key Laboratory of Neuropsychiatric Diseases and College of Pharmaceutical Sciences, Soochow University, Suzhou 215123, China
[d] Laboratory for Translational Genetics, Department of Human Genetics, KU Leuven, Leuven, Belgium
[e] VIB Center for Cancer Biology, Leuven, Belgium
[f] Systems Biology Ireland, School of Medicine, University College Dublin, Belfield, Dublin 4, Ireland
[g] Mass Spectrometry Resource, Conway Institute of Biomolecular & Biomedical Research, University College Dublin 4, Ireland

ARTICLE INFO

Keywords:
Amyotrophic lateral sclerosis (ALS)
Transfer RNA-derived stress-induced RNA (tiRNAs)
Small non-coding RNA (sncRNA)
Angiogenin (ANG)
Stress response

ABSTRACT

tRNA-derived stress-induced RNAs (tiRNAs) are a new class of small non-coding RNA that have emerged as important regulators of cellular stress responses. tiRNAs are derived from specific tRNA cleavage by the stress-induced ribonuclease angiogenin (ANG). Loss-of-function mutations in the *ANG* gene are linked to amyotrophic lateral sclerosis (ALS), and elevated levels of specific tiRNAs were recently identified in ALS patient serum samples. However, the biological role of tiRNA production in neuronal stress responses and neurodegeneration remains largely unknown. Here, we investigated the genome-wide regulation of neuronal stress responses by a specific tiRNA, 5'tiRNA$^{Gly\text{-}GCC}$, which we found to be upregulated in primary neurons exposed to ALS-relevant stresses and in the spinal cord of three ALS mouse models. Whole-transcript RNA sequencing and label-free mass spectrometry on primary neurons transfected with a synthetic mimic of 5'tiRNA$^{Gly\text{-}GCC}$ revealed predominantly downregulated RNA and protein levels, with more pronounced changes in the proteome. Over half of the downregulated mRNAs contained predicted 5'tiRNA$^{Gly\text{-}GCC}$ binding sites, indicating that this tiRNA may silence target genes via complementary binding. On the proteome level, we observed reduction in proteins involved in translation initiation and ribosome assembly, pointing to inhibitory effects on translation. Together, these findings suggest that 5'tiRNA$^{Gly\text{-}GCC}$ is an ALS-associated tiRNA that functions to fine-tune gene expression and supress protein synthesis as part of an ANG-induced neuronal stress response.

1. Introduction

Amyotrophic lateral sclerosis (ALS) is a devastating, highly heterogeneous but uniformly fatal neurodegenerative disease for which treatment options are still lacking. The disease is characterized by progressive degeneration of upper and lower motor neurons in the cerebral cortex and spinal cord, leading to muscle weakness, paralysis and eventually death, usually within 3–5 years from symptom onset (Brown and Al-Chalabi, 2017). ALS displays a considerable clinical, pathophysiological and genetic overlap with several other neurodegenerative diseases, particularly frontotemporal dementia (FTD) (Burrell et al., 2011). Despite recent advances in genetic and molecular studies, the aetiology and pathogenesis of the disease remain poorly understood, delaying the development of disease-modifying treatments.

Accumulating evidence suggests that aberrant RNA processing in response to stress is a key contributor to the pathogenesis of neurodegenerative diseases, especially ALS and FTD (Wolozin and Ivanov, 2019). In recent years, a new class of functional small non-coding RNAs

* Corresponding author at: Department of Physiology and Medical Physics, Royal College of Surgeons in Ireland, 123 St Stephen's Green, Dublin 2, Ireland.
E-mail address: prehn@rcsi.ie (J.H.M. Prehn).
[1] Current address: Department of Biosciences, School of Science and Technology, Nottingham Trent University, NG11 8NS, United Kingdom.

https://doi.org/10.1016/j.expneurol.2024.115128
Received 11 November 2024; Received in revised form 16 December 2024; Accepted 19 December 2024
Available online 22 December 2024

(sncRNAs) known as 'transfer RNA-derived stress-induced RNAs' ('tiRNAs'), have emerged as crucial regulators of cellular stress responses (Li et al., 2018). tiRNAs are derived from specific tRNA cleavage by the stress-induced ribonuclease angiogenin (ANG). Under conditions of cellular stress, ANG cleaves mature tRNA in the anticodon loop which gives rise to two subclasses of tiRNAs; 5'tiRNAs and 3'tiRNAs of approximately 30–40 nucleotides in length (Fu et al., 2009; Yamasaki et al., 2009; Saikia et al., 2012). Of note, ANG is a neuroprotective factor and several loss-of-function mutations in the *ANG* gene have been identified in both sporadic and familial cases of ALS (Greenway et al., 2006; Kieran et al., 2008; Sebastià et al., 2009; Subramanian et al., 2007), suggesting that aberrant tiRNA production may lead to neurodegeneration. Furthermore, specific 5'tiRNAs containing G-quadruplex (G4) structures associated with ALS and FTD have been reported to protect human motor neurons against various ALS-relevant stresses (Ivanov et al., 2014). Recently, our group and others reported upregulated levels of specific 5'tiRNAs, including 5'tiRNA$^{Val\text{-}CAC}$ and 5'tiRNA$^{Val\text{-}AAC}$, in serum samples from ALS patients (Hogg et al., 2020; Joilin et al., 2020). Interestingly, levels of 5'tiRNA$^{Val\text{-}CAC}$ were also elevated in the spinal cord of SOD1^{G93A} ALS transgenic (TG) mice at symptom onset and correlated with a slower disease progression in both this model and in the ALS patient serum samples (Hogg et al., 2020). Collectively, these findings suggest that 5'tiRNAs hold potential as prognostic biomarkers for ALS and may be part of an ANG-mediated neuroprotective stress response.

In addition to the potential of tiRNAs as disease biomarkers, it is becoming increasingly evident that this novel group of sncRNAs are important regulators of a wide range of biological processes across all domains of life (Li et al., 2018). Early studies reported that a subset of 5'tiRNAs inhibit global protein synthesis and promote formation of stress granules (SGs), membraneless cytoplasmic foci which transiently store translationally inactive mRNA and RNA binding proteins (RBPs), by interfering with the assembly of the translation initiation machinery (Yamasaki et al., 2009; Ivanov et al., 2011; Emara et al., 2010). Subsequent studies have corroborated these findings and provided further evidence that tiRNAs regulate various stages of gene expression, such as regulation of mRNA stability (Goodarzi et al., 2015; Jehn et al., 2020), inhibition of translation and regulation of ribosome biogenesis (Goncalves et al., 2016; Fricker et al., 2019; Kim et al., 2019; Lyons et al., 2020). Two independent studies implicated tiRNA-mediated genome-wide regulation of gene expression during early embryonic development. Several 5'tiRNAs, particularly 5'tiRNA$^{Gly\text{-}GCC}$, were found enriched in mouse sperm cells and altered offspring gene expression by binding to promoter regions in the zygote's genome (Chen et al., 2016; Sharma et al., 2016). Furthermore, a recent study demonstrated that two specific 5'tiRNAs, 5'tiRNA$^{Gly\text{-}GCC}$ and 5'tiRNA$^{Glu\text{-}CTC}$, can silence gene expression in human HEK293 (Jehn et al., 2020). Additionally, 5'tiRNA$^{Gly\text{-}GCC}$ was identified as one of the most abundantly expressed tiRNAs in both human and mouse brain tissue (Jehn et al., 2020), and its expression has been shown to increase in various cell lines under stress conditions (Elkordy et al., 2018; Sanadgol et al., 2022). Taken together, these studies highlight a potential role for 5'tiRNAs, and 5'tiRNA$^{Gly\text{-}GCC}$ in particular, in the regulation of gene expression. However, the effects of tiRNAs on global gene and protein expression in neuronal stress responses and neurodegeneration remain unexplored. Given 5'tiRNA$^{Gly\text{-}GCC}$ regulatory role and its abundance in brain tissue, we sought to investigate its dysregulation in ALS models as well as the systems-wide impact of this tiRNA during neuronal stress conditions. Using RNA sequencing (RNA-seq) and quantitative proteomics, we analyzed transcriptomic and proteomic changes in primary neurons transfected with synthetic mimics of 5'tiRNA$^{Gly\text{-}GCC}$, identifying biological processes and pathways potentially regulated by tiRNAs in neuronal stress responses.

2. Material and methods

2.1. Animals

All animal work was performed in accordance with the European Union Directive (2010/63/EU) with ethical approval by the RCSI Research Ethics Committee (REC1122 and TH007), and under sequential licences from the Health Products Regulatory Authority (AE19127/P004 and AE19127/P054), Dublin, Ireland. All animals were housed in a climate-controlled environment on a 12 h light/dark cycle with food and water supplied ad libitum.

C57BL/6JOlaHsd mice were purchased from Envigo, UK. TDP-43^{A315T} hemizygous mice on a congenic C57BL/6 background (B6.Cg-Tg (Prnp-TARDBP*A315T)95Balo/J), were purchased from The Jackson Laboratory (Bar Harbor, Maine, USA) and originally generated in the laboratory of Dr. Baloh (Wegorzewska et al., 2009). A TDP-43^{A315T} colony was maintained using a protocol that ensures development of symptomatic motor dysfunction, and were monitored daily from postnatal day (PND) 80 for development of symptoms (Coughlan et al., 2016). Only male TDP-43^{A315T} mice were analyzed, as female mice display variable disease penetrance (Hogg et al., 2018). SOD1^{G93A} mice (C57B6.Cg-Tg (SOD1G93A)1Gur/J mice were purchased from The Jackson Laboratory (Bar Harbor, Maine) and originally generated in the laboratory of Professor Siddique (Gurney et al., 1994). The SOD1G93A transgene copy number was verified as stable in breeding males from the colony (Hogg et al., 2018). The FUS (1–359) mice were originally generated in the laboratory of Professor Buchman (Shelkovnikova et al., 2013) and were rederived at the Institute of Molecular Genetics ASCR, Prague, Czech Republic as a congenic line on the C57Bl/6 background. Mice were genotyped by PCR, and aged to specific timepoints for tissue collection which were different for each strain. Pre-symptomatic samples and symptom onset samples were collected, see figure legends for specific timepoints. TG and non-transgenic (WT) littermates were housed together with 3–5 mice per cage.

2.2. Tissue collection

Mice were terminally anesthetized with sodium pentobarbitone, and after the absence of reflexes were confirmed, transcardially perfused with PBS. Spinal cords were dissected and snap frozen in liquid nitrogen, and samples were stored at −80 °C until used for RNA extraction.

2.3. Preparation of mouse primary cortical neurons

Cultures of primary cortical neurons were prepared from C57BL/6JOlaHsd mouse embryos at embryonic day 16 (E16) as previously described (Concannon et al., 2010). Dissociated cortical neurons were resuspended in plating medium consisting of MEM (Gibco) supplemented with 10 % horse serum (Gibco), 10 % fetal bovine serum (Sigma-Aldrich), 0.5 mM GlutaMAX (100×, Gibco), 1 % Penicillin-Streptomycin (10,000 U/ml, Gibco), 0.6 % (*w/v*) D-glucose (Sigma-Aldrich), 1 mM pyruvic acid (Gibco) and 0.22 % (w/v) $NaHCO_3$ (Sigma-Aldrich). Cells were seeded onto poly-L-lysine-coated (0.1 mg/ml, Sigma-Aldrich) 6-well plates at a density of 1.4×10^6 cells/well or onto poly-L-lysine-coated (0.1 mg/ml) glass coverslips in 24-well plates at a density of 3.5×10^5 cells/well and cultured in a controlled humified incubator at 37 °C and with 5 % CO_2. 4 h after plating the cells, the plating medium was replaced with fresh serum-free Neurobasal plus medium (Gibco) supplemented with 0.5 mM GlutaMAX (100×), 10 μg/ml Gentamicin and 1× B27 plus supplement (50×) (Gibco). On day in vitro (DIV 1), cultures were treated with 1 μM cytosine arabinoside (AraC, Sigma-Aldrich) to inhibit growth of non-neuronal cells. Half media changes were performed every three to four days until the cells were used for further experiments.

2.4. Cell culture treatments

To induce proteasomal stress, cultures of mouse primary cortical neurons (DIV 9) were treated with either 50 nM proteasome inhibitor epoxomicin (Sigma-Aldrich) or vehicle control (0.1 % DMSO) for 24 h at 37 °C and 5 % CO_2. For acute oxidative stress induction, cultures of mouse primary cortical neurons (DIV 9) were treated with 500 μM sodium arsenite (SA, Sigma-Aldrich) for 1 h followed by 24 h recovery in the original conditioned culture medium at 37 °C and 5 % CO_2. Untreated cells were used as control. To induce excitotoxicity, the primary neurons were treated with two concentrations of glutamate (0.5 mM and 1 mM) (Sigma-Aldrich) for 30 min at 37 °C and 5 % CO_2. Untreated cells were used as control.

2.5. tiRNA transfection

A synthetic mimic of endogenous 5'tiRNA$^{Gly\text{-}GCC}$ and a non-targeting scrambled 5'tiRNA sequence (scrambled control) were synthesised and purified by Integrated DNA Technologies (IDT). The mimics contained a phosphorylated 3′-end and a biotinylated 5′-end and the sequences were as follows: 5'tiRNA$^{Gly\text{-}GCC}$, 5'Bio-GCAUUGGUGGUUCAGUGGUAGAAUUCUCGCCUGC-3'Phospho; and scrambled control, 5'Bio-UGUGAGUCACGUGAGGGCAGAAUCUGCUC-3'Phospho. On DIV 8, cultures of mouse primary cortical neurons were transfected with synthetic 5'tiRNA$^{Gly\text{-}GCC}$ mimic or scrambled control using NeuroMag transfection reagent and protocol (Oz Biosciences). Briefly, 100 nM synthetic tiRNA mimic or control was mixed with NeuroMag reagent (3.5 μl/well for 24-well plates and 14 μl/well for 6-well plates) in serum-free Neurobasal plus medium (final volume of 100 μl/well in 24-well plates and 200 μl/well in 6-well plates, Gibco) without supplements and incubated for 15–20 min at room temperature (RT) to allow formation of tiRNA/NeuroMag complexes. Then, the appropriate amount of conditioned media was discarded from the cells and equal volume of transfection mix was added dropwise onto the cells. The culture plate was placed on a magnetic plate (Oz Biosciences) for 20 min in a humified incubator at 37 °C and 5 % CO_2. Following transfection, neurons were cultured under standard conditions for 24 h until further use.

2.6. Immunocytochemistry

Immunocytochemistry was performed on tiRNA mimic-transfected primary cortical neurons grown on coverslips in standard 24-well plates or 35 mm glass bottom dishes (Ibidi, #81158). Cells were fixed with 4 % paraformaldehyde for 15 min, permeabilised in ice-cold 0.1 % Triton X-100/PBS for 5 min, blocked in 5 % (*w/v*) BSA/0.1 % Triton X-100/PBS for 1 h at RT, and incubated with rabbit polyclonal anti-MAP2 antibody (1:500, Abcam, #ab32454) and mouse monoclonal anti-G3BP1 (1:800, BD Bioscience, #AB_398438) overnight at 4 °C. Following primary antibody incubation, cells were incubated with an Alexa Fluor® Plus 555-conjugated donkey anti-rabbit secondary antibody (1:1000, Invitrogen, # A32794), an Alexa Fluor® Plus 488-conjugated donkey anti-mouse secondary antibody (1:1000, Invitrogen, #A21202), an Alexa Fluor® 647-conjugated streptavidin (1:500, Invitrogen, #S32357) and 1 μg/ml Hoechst 33342 nuclear stain (Invitrogen) for 2 h at RT. Coverslips were mounted using ProLong Diamond Antifade Mountant (Invitrogen) and *Z*-stack images were acquired using a confocal Zeiss LSM 710 microscope with a 40× oil immersion objective (EC Plan-Neofluar 40×/1.30 Oil DIC M27, Zeiss). Dish samples were acquired using confocal Zeiss LSM 980 microscope with a 40× oil immersion objective (EC Plan-Neofluar 40×/1.30 Oil DIC M27, Zeiss). Five random field of views per coverslip or dish were imaged (1 coverslip or dish/independent experiment) and were analyzed using ImageJ (U.S. National Institutes of Health). To calculate transfection efficiency of synthetic tiRNA mimics, thresholds were applied to single *Z*-stack slices at the level of the nucleus to create masks of all MAP2-positive cells, and then the Alexa Fluor® 647 mean fluorescence intensity (MFI) was measured in the MAP2-masked area. All confocal microscope and ImageJ analysis settings were kept constant between experiments.

2.7. RNA extraction

Total RNA was extracted from mouse primary cortical neurons using Trizol reagent (Invitrogen) according to manufacturer's instructions. Briefly, samples were lysed and homogenised in Trizol reagent and incubated for 5 min at RT. Phase separation was performed by adding chloroform (Sigma-Aldrich) and shaking the samples for 15 s. The samples were incubated for 3 min at RT and then centrifuged at 12000 x*g* for 15 min at 4 °C. The upper aqueous phase was transferred into a new tube and an equal volume of isopropanol (Sigma-Aldrich) was added. Samples were incubated overnight at −20 °C and then centrifuged at 12000 x*g* for 15 min at 4 °C. The RNA pellets were washed with 75 % ethanol (Sigma-Aldrich), vortexed briefly and then centrifuged at 7500 x*g* for 10 min at 4 °C. The RNA pellets were air-dried for 10 min at RT and then resuspended in 20 μl RNase-free water containing 1 μl RNaseOUT RNase inhibitor (Invitrogen). The samples were incubated for 10 min at 65 °C, cooled on ice and spun down. RNA was extracted from mouse tissue using the Qiagen miRNeasy kit (Qiagen) according to the manufacturer's instructions, and eluted in 40 μl RNase-free water containing 1 μl RNaseOUT RNase inhibitor (Invitrogen). RNA purity and yield was analyzed using a Nanodrop 2000 spectrophotometer (Thermo Scientific).

2.8. RNA secondary structure prediction

The sequences of mature tRNA$^{Gly\text{-}GCC}$ and 5'tiRNA$^{Gly\text{-}GCC}$ were extracted from the GtRNAdb (Chan and Lowe, 2009; Chan and Lowe, 2016) and a small RNA-seq study performed previously in the lab (Hogg et al., 2020). The minimum free energy (mfe) predicted secondary structures of tRNA$^{Gly\text{-}GCC}$ and 5'tiRNA$^{Gly\text{-}GCC}$were calculated using the ViennaRNA RNAfold Server (Lorenz et al., 2011).

2.9. TaqMan RT-qPCR

A custom TaqMan™ Small RNA Assay (Applied Biosystems) for 5'tiRNA$^{Gly\text{-}GCC}$ (5′- GCAUUGGUGGUUCAGUGGUAGAAUUCUCGCCUGC-3′, Assay ID available upon request) was designed, validated and used in two-step RT-qPCR as previously described (Hogg et al., 2020). Briefly, 100 ng DNase I-treated total RNA was reverse transcribed using TaqMan™ MicroRNA Reverse Transcription Kit (Applied Biosystems) and qPCR reactions were performed in triplicate on a QuantStudio™ 5 Real-Time PCR System (Applied Biosystems). tiRNA levels were normalised to U6 small nuclear RNA (Applied Biosystems, assay ID 001973) and tiRNA expression relative to control samples was calculated using the $2_t^{-\Delta\Delta C}$ method (Livak and Schmittgen, 2001).

2.10. RNA-sequencing

Whole transcript RNA-seq was performed by VIB-KU Leuven on total RNA extracted from primary neurons transfected with either 5'tiRNA$^{Gly\text{-}GCC}$ mimic or scrambled control ($n = 5$ independent experiments) using the KAPA stranded mRNA-seq Kit (Roche) as previously described (Lucantoni et al., 2021). Transcriptome profiles were created using an existing in-house bioinformatics pipeline (VIB-KU Leuven). In brief, following removal of optical duplicates using Clumpify (Bushnell et al., 2017), the FASTQ sequencing reads were mapped to the mouse reference genome using STAR 2.6 (Dobin et al., 2012), and SAM files were created. SAMtools (Li et al., 2009) was used to convert SAM files into binary format BAM. HTSeq-Count (Anders et al., 2014) was used to preprocess the BAM files for downstream analyses by counting the number of reads mapping to the genes. Differential gene expression analysis was performed in R v3.4.4 (R Core Team, 2013) using the DeSeq2 package

from Bioconductor (Love et al., 2014). Genes with an unadjusted *p*-value of less than 0.05 were considered significant as this was an exploratory study with a small sample size. Top differentially expressed (DE) genes were determined using a cut-off criteria of unadjusted *p*-value <0.05 and $|\log_2 \text{fold change}| > 1$.

2.11. Computational prediction of 5'tiRNA$^{Gly\text{-}GCC}$ target interaction

RNAhybrid version 2.1.2 (Krüger and Rehmsmeier, 2006) was used to identify potential binding sites on the DE genes identified in the RNA-seq data. We used protein coding sequences for 601 of the 604 DE mRNAs (3 mRNAs have retired status on Ensembl) and lncRNA sequences for 39 DE lncRNAs from GENCODE release M25 (GRCm38.p6) as the target sequences and 5'tiRNA$^{Gly\text{-}GCC}$ as the query sequence. RNAhybrid uses extreme value distribution to estimate the *p*-values, we used 3utr_human option for this. Predicted hybridisations with mfe less than −25 and *p*-value less than 0.05 were considered as probable binding sites. We obtained the graphical representations of the binding interactions from the RNAhybrid website (https://bibiserv.cebitec.uni-bielefeld.de/rnahybrid) (Krüger and Rehmsmeier, 2006).

2.12. Quantitative proteomics

Label-free quantitative proteomics analysis was performed as described before (Matveeva et al., 2023) on protein samples from mouse primary cortical neurons transfected with either 5'tiRNA$^{Gly\text{-}GCC}$ mimic or scrambled control ($n = 5$ independent experiments). Briefly, cultured neurons were lysed in 2 % SDS lysis buffer (50 mM Tris-HCl, pH 7.5, 2 % SDS, all Sigma-Aldrich) containing Roche cOmplete™ Protease Inhibitor Cocktail and Roche PhosSTOP™ tablets phosphatase inhibitors mix (Roche). Lysates were sonicated on a Bioruptor Pico (Diagenode), incubated at 95 °C for 5 min and then centrifuged at 14,000 rpm for 7 min at 4 °C to remove cellular debris. Total protein concentration was quantified using a Micro BCA protein assay (Thermo Scientific). Samples were further processed in Dr. Matallanas' laboratory using filter-aided sample preparation (FASP), a method that allows on-filter digestion of solubilised proteins and detergent removal using ultrafiltration devices (Wiśniewski et al., 2009). The peptide mixtures were purified, enriched and anion-exchanged fractionated using C18-StageTips (Empore). Briefly, C18-StageTips and solvents were prepared as previously described (Rappsilber et al., 2007), activated with 50 % acetonitrile (AcN)-0.1 % trifluoroacetic acid (TFA) and washed with 0.1 % TFA. 10 μg of Trypsin digests were loaded onto the tips, washed twice with 0.1 % TFA, and eluted in 40 % AcN-0.1 % TFA. Then, samples were evaporated in a CentriVap Concentrator and resuspended in 0.1 % TFA prior to liquid chromatography coupled to tandem mass spectrometry (LC-MS/MS) analysis.

LC-MS/MS analysis was performed by the UCD Conway Institute Mass Spectrometry Core Facility. Tryptic peptide samples were run on a Bruker timsTof Pro mass spectrometer coupled to a Bruker NanoElute nano-lc chromatography system (Bruker). Tryptic peptides were resuspended in 0.1 % formic acid. To evaluate the reproducibility of LC-MS/MS, 2 pmol Hi3 standard consisting of six synthetic control peptides was added to each sample immediately before injection. Each sample was loaded onto an Aurora Series UHPLC column (25 cm × 75 μm ID, 1.6 μm C18) (Ionopticks) and separated with an increasing acetonitrile gradient over 60 min at a flow rate of 250 nl/min at 45 °C. Chromatography buffer A was 99.9 % water, 01 % formic acid and buffer B was 99.9 % acetonitrile, 0.1 % formic acid (all solvents were LCMS grade). The mass spectrometer, Bruker timsTof Pro, was operated in positive ion mode with a capillary voltage of 1500 V, dry gas flow of 3 l/min and a dry temperature of 180 °C. All data was acquired with the instrument operating in trapped ion mobility spectrometry (TIMS) mode. Trapped ions were selected for MS/MS using parallel accumulation serial fragmentation (PASEF). A scan range of (100–1700 m/z) was performed at a rate of 10 PASEF MS/MS frames to 1 MS scan with a cycle time of 1.15 s. One technical replicate and five biological replicates were run for each sample.

The resulting LC-MS/MS data were analyzed using the search engine MaxQuant version 1.6.17.0 (Cox and Mann, 2008). The raw files were searched against the *Mus musculus* subset of the Uniprot Swissprot database (reviewed) using specific parameters for TIMS data dependent acquisition (TIMS DDA). Each peptide used for protein identification met specific MaxQuant parameters, i.e., only peptide scores that corresponded to a FDR of 0.01 were accepted from the MaxQuant database search. The normalised protein intensity of each identified protein was used for label-free quantification (LFQ). Match between runs and intensity-based absolute quantification (iBAQ) were also selected. Preliminary iBAQ *LC-MS/MS* quantities were processed in the Perseus environment v1.6.7.0 (Tyanova et al., 2016). Processing included: deletion of proteins matching to reverse database and contaminants; relative iBAQ (riBAQ) normalization (Krey et al., 2014; Krey et al., 2018); exclusion of proteins identified by site, $\log_2$ transformation and filtration for proteins with Andromeda score above 40 in order to exclude low confidence identifications. Further analysis was continued in the R environment (R Core Team, 2013) with *limma* package v3.40.6 (Ritchie et al., 2015). DE proteins were identified by paired moderated *t*-test. The significance level was set to unadjusted *p*-value <0.05 as this was an exploratory study with a small sample size (Pascovici et al., 2016). Top DE proteins were determined using a cut-off criteria of unadjusted *p*-value <0.05 and $|\log_2 \text{fold change}| > 1$.

2.13. Functional enrichment analysis

Gene ontology (GO) (Ashburner et al., 2000), Kyoto encyclopedia of genes and genomes (KEGG) (Kanehisa and Goto, 2000; Kanehisa, 2019; Kanehisa et al., 2021), Reactome (Gillespie et al., 2022) and WikiPathways (Martens et al., 2021) analysis of identified DE mRNAs, DE proteins and hub genes was carried out using EnrichR (Chen et al., 2013; Kuleshov et al., 2016), and an adjusted *p*-value cut-off of below 0.05 was used to filter results. Treemaps of enriched biological processes were created in R v4.0.3 (R Core Team, 2013) using the Bioconductor package rrvgo (Sayols, 2020).

2.14. Protein-protein interaction network analysis

Protein-protein interaction (PPI) networks of the DE proteins were constructed and analyzed using the Cytoscape platform v3.9.1 (Shannon et al., 2003). Briefly, PPI networks were retrieved from the STRING database v11.5 (Szklarczyk et al., 2019) and then visualized and analyzed using the Cytoscape stringApp (Doncheva et al., 2019). The interaction score threshold was set to 0.7 (high confidence level) and a PPI enrichment *p*-value cut-off of <0.05 was considered significant. PPI network clusters (modules) were identified using the Cytoscape MCODE app v2.0.0 (Bader and Hogue, 2003) with default cluster finding parameters (Degree cutoff ≥2; Node score cutoff ≥0.2, K-Core 2 and Max Depth = 100). Hub genes in the PPI network were identified using the Cytoscape app cytoHubba (Chin et al., 2014) and the top 20 nodes were ranked by the Maximal Clique Centrality (MCC) algorithm. KEGG pathway analysis of the identified modules was performed using the StringApp (cut-off criteria: FDR-adjusted *p*-value <0.05).

2.15. Statistical analysis

Statistical analyses were performed using Graphpad Prism v9.3.1 (GraphPad Software Inc., San Diego, California, USA) or R v3.4.4/4.0.3 (R Core Team, 2013). The statistical approaches for RNA-seq, proteomics and functional enrichment analyses are detailed in respective methods sections above. The Shapiro-Wilk test was performed to assess normality of TaqMan RT-qPCR data. Normally distributed data were plotted as mean ± standard error mean (SEM) and analyzed by two-tailed *t*-tests with the significance level set to *p*-value <0.05. The

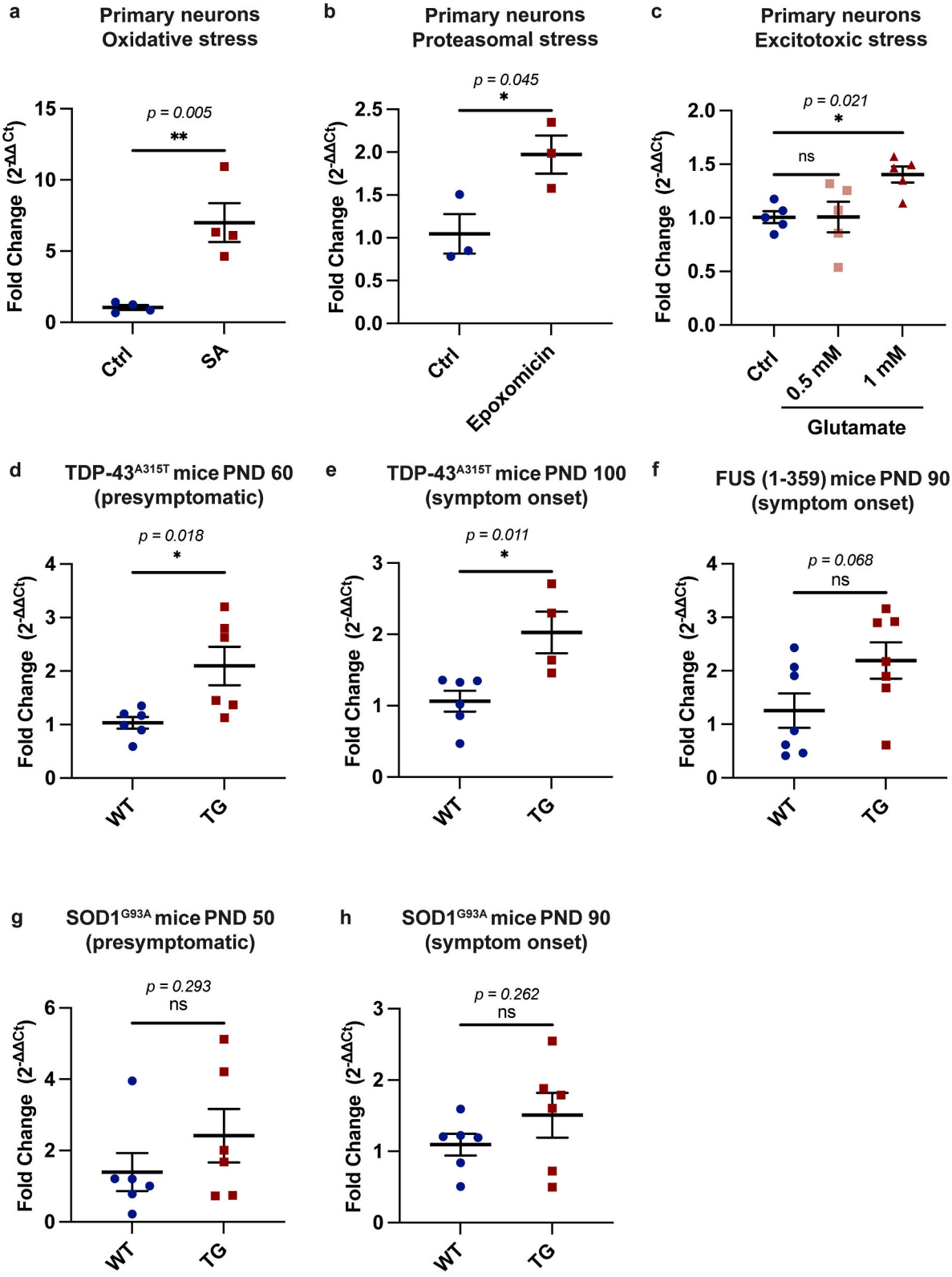

Fig. 1. 5'tiRNA$^{Gly\text{-}GCC}$ levels are increased in cellular models of ALS-relevant stresses and in ALS mouse models. A-C TaqMan RT-qPCR analysis of 5'tiRNA$^{Gly\text{-}GCC}$ levels relative to U6 snRNA in mouse primary cortical neurons exposed to A sodium arsenite (SA)-induced oxidative stress compared to control (Ctrl), B epoxomicin-induced proteasomal stress compared to Ctrl, and C glutamate-induced excitotoxic stress compared to Ctrl. D—H TaqMan RT-qPCR analysis of 5'tiRNA$^{Gly\text{-}GCC}$ levels in spinal cord RNA relative to U6 snRNA of D TDP-43^{A315T} transgenic (TG) mice at postnatal day (PND) 60 (presymptomatic) compared to wild type (WT) littermates, E TDP-43^{A315T} TG mice at PND 100 (symptom onset) compared to WT littermates, F FUS (1–359) mice at PND 90 (symptom onset) compared to WT littermates, G SOD1^{G93A} TG mice at PND 50 (presymptomatic) compared to WT, and H SOD1^{G93A} TG mice at PND 90 (symptom onset) compared to WT littermates. Data are mean +/− SEM from $n = 3$–6 independent experiments/mice as indicated by dots; *$p < 0.05$; **$p < 0.01$; ns = not significant, two-tailed *t*-test (A-B, D—H) or One-Way Anova followed by Dunnett's multiple comparison test (C).

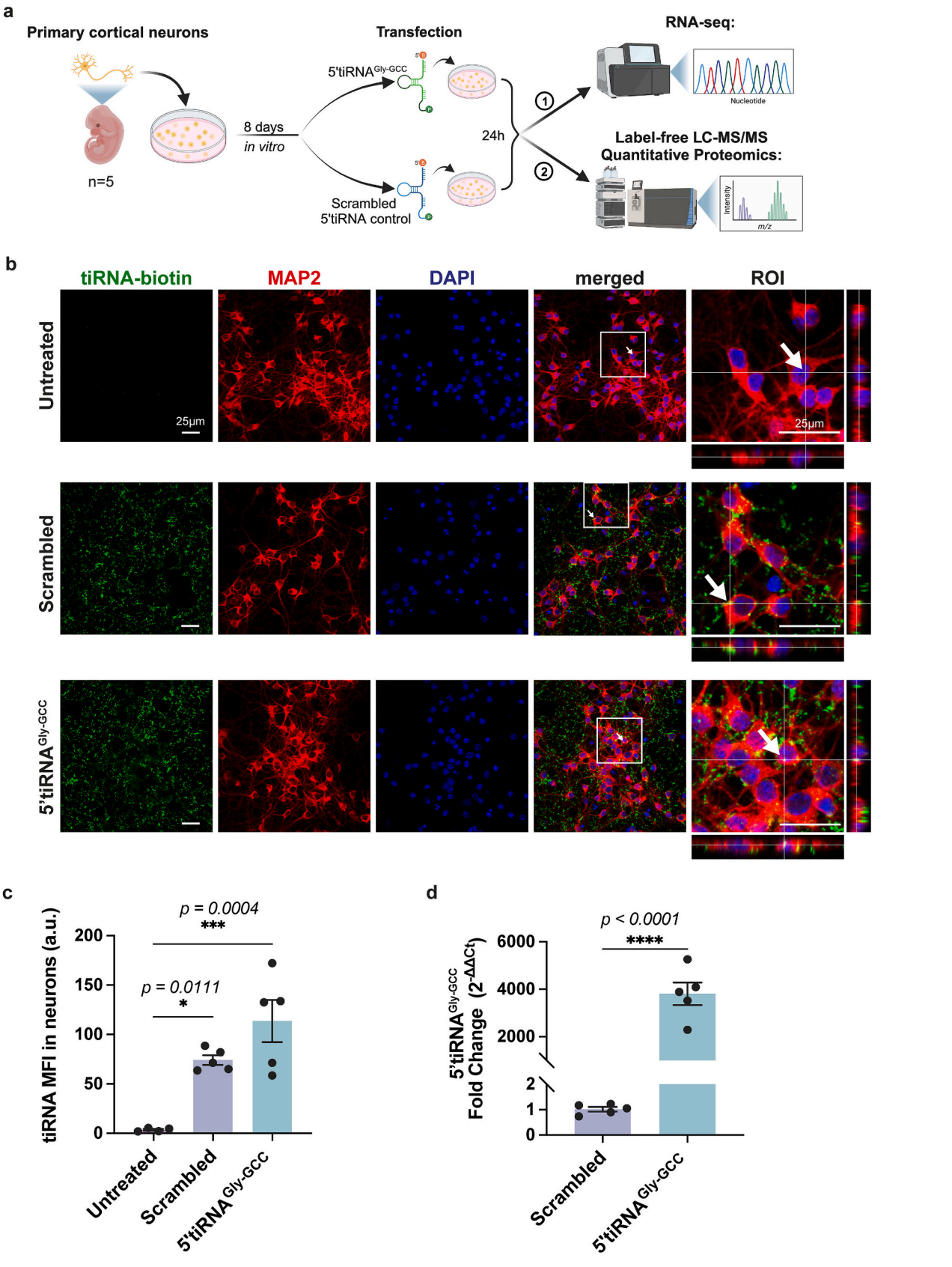

(caption on next page)

Fig. 2. Sample preparation for transcriptomics and proteomics analyses of 5'tiRNA$^{Gly\text{-}GCC}$-transfected primary neurons. A Sample preparation workflow. Cultures of mouse primary cortical neurons (DIV 8) were transfected with synthetic biotin-labelled mimics of either 5'tiRNA$^{Gly\text{-}GCC}$ or a scrambled 5'tiRNA control for 24 h using NeuroMag transfection technology. Whole-transcript RNA-seq and label-free LC-MS/MS quantitative proteomics analysis was performed on the tiRNA-mimic and scrambled control-transfected neurons ($n = 5$ per condition). Schematic created with BioRender.com. B Representative confocal z-stack images of intraneuronal tiRNA-biotin levels (green; stained with fluorochrome-conjugated streptavidin) 24 h post-transfection. Neuronal marker MAP2 is shown in red and Hoechst nuclear counterstain is shown in blue. Arrows indicate cells selected as origin for orthogonal views. $n = 10$ independent experiments ($n = 5$ for proteomics and $n = 5$ for RNA-seq). Scale bars, 25 μm. ROI; region of interest. C tiRNA mean fluorescence intensity (MFI, a.u., arbitrary unit) measured in the cytoplasm of neurons (MAP2-masked area). D TaqMan RT-qPCR analysis of 5'tiRNA$^{Gly\text{-}GCC}$ intracellular levels relative to U6 snRNA in mouse primary cortical neurons transfected with synthetic mimic of 5'tiRNA$^{Gly\text{-}GCC}$ relative to scrambled control. Data are mean +/− SEM from $n = 4$–5 independent experiments as indicated by dots; $^{*}p < 0.05$, $^{***}p < 0.001$, $^{****}p < 0.0001$. One-way ANOVA followed by Tukey's multiple comparison test (C), Two-tailed *t*-test (D). (For interpretation of the references to colour in this figure legend, the reader is referred to the web version of this article.)

number of technical and biological replicates, the statistical tests used, and the significance are indicated in the figure legends.

3. Results

3.1. Levels of 5'tiRNA$^{Gly\text{-}GCC}$ are upregulated in primary neurons exposed to ALS-relevant stresses and in the spinal cord of transgenic ALS mouse models at early stages of the disease

Stresses proposed to be involved in ALS include excitotoxicity, endoplasmic reticulum stress, oxidative stress and proteasomal stress (Taylor et al., 2016; Mejzini et al., 2019). To assess whether disease-relevant stresses alter neuronal levels of 5'tiRNA$^{Gly\text{-}GCC}$, cultures of mouse cortical neurons were exposed to SA-induced oxidative stress, epoxomicin-induced proteasomal stress, and glutamate-induced excitotoxic stress. The intracellular levels of 5'tiRNA$^{Gly\text{-}GCC}$ compared to those in control samples were quantified using a custom small TaqMan RT-qPCR assay developed by our group to specifically recognize 5'tiRNA$^{Gly\text{-}GCC}$ and discriminate between the tiRNA and full length tRNA, as previously validated by northern blotting (Hogg et al., 2020). The sequences and secondary structures of 5'tiRNA$^{Gly\text{-}GCC}$ and its parental tRNA are shown in Supplementary Fig. S1. Exposure to acute SA-mediated oxidative stress resulted in a robust upregulation (~7-fold) of intracellular 5'tiRNA$^{Gly\text{-}GCC}$ (Fig. 1a). A significant increase in 5'tiRNA$^{Gly\text{-}GCC}$ levels (~2-fold) was also observed in the epoxomicin-treated neurons compared to control-treated neurons (Fig. 1b). A moderate increase (~1.5-fold) was also evident in neuronal cultures exposed to 1 mM glutamate compared to untreated control cultures (Fig. 1c), providing further evidence for upregulated tiRNA$^{Gly\text{-}GCC}$ production during several ALS-related neuronal stress conditions.

To investigate tiRNA production in a more disease-relevant context, we measured 5'tiRNA$^{Gly\text{-}GCC}$ in the lumbar spinal cord of mice from three different TG mouse models of ALS at an early stage of the disease, including the TDP-43^{A315T} model of ALS and FTD, the FUS (1–359) ALS model and the SOD1^{G93A} ALS model of slow disease progression. We identified significantly elevated levels of this tiRNA (~2-fold) at the presymtomatic stage (PND 60) and at symptom onset (PND 100) in TG mice from the TDP-43^{A315T} model compared to WT littermates (Fig. 1d-e). Elevated, although not statistically significant, levels of 5'tiRNA$^{Gly\text{-}GCC}$ were also observed at symptom onset in FUS (1–359) TG mice compared to WT littermates (Fig. 1f). Levels of 5'tiRNA$^{Gly\text{-}GCC}$ were slightly increased, but no statistically significant difference was observed, in TG SOD1^{G93A} mice compared to WT littermates (Fig. 1h). Taken together, these findings link increased 5'tiRNA$^{Gly\text{-}GCC}$ production to neuronal stress that occurs before overt symptoms develop in multiple TG mouse models of ALS.

3.2. Transcriptomic and proteomic analyses of 5'tiRNA$^{Gly\text{-}GCC}$ transfected primary neurons

Having established that 5'tiRNA$^{Gly\text{-}GCC}$ is upregulated in disease-relevant in vitro and in vivo models of ALS, we next sought to explore its systems-wide effects on gene expression and protein expression in primary neurons. To this end, we designed synthetic oligonucleotide mimics of endogenous 5'tiRNA$^{Gly\text{-}GCC}$ and a scrambled tiRNA control, and then performed whole-transcript RNA-seq and label-free quantitative proteomics on primary neurons transfected with the mimics (Fig. 2a). Before commencing omics studies, we performed immunocytochemistry to confirm efficient transfection of both the 5'tiRNA and scrambled control mimics into neurons. Following 24 h of transfection, the mimics were endocytosed by primary neurons where they accumulated mainly in the cytoplasm and dendrites as documented by confocal z-stack imaging and co-staining with a MAP2 antibody (Fig. 2b). Mimics also formed extracellular aggregates. The intraneuronal tiRNA signal was higher in the cultures transfected with 5'tiRNA$^{Gly\text{-}GCC}$ or scrambled control compared to the non-transfected cultures, confirming successful internalisation of the mimics (Fig. 2c). There was no statistical difference in intraneuronal 5'tiRNA$^{Gly\text{-}GCC}$ immunofluorescence compared to scrambled control. Co-staining with a G3BP1 antibody suggested that internalised 5'tiRNA$^{Gly\text{-}GCC}$ did not induce stress granule formation or co-localise to SGs (Supplementary Fig. S2). To further validate efficient transfection, the intracellular levels of 5'tiRNA$^{Gly\text{-}GCC}$ were quantified using TaqMan RT-qPCR assays which confirmed significantly higher levels of 5'tiRNA$^{Gly\text{-}GCC}$ in the tiRNA-transfected neurons compared to scrambled controls (Fig. 2d).

3.3. Transfection of 5'tiRNA$^{Gly\text{-}GCC}$ fine-tunes gene expression in primary neurons

To investigate 5'tiRNA$^{Gly\text{-}GCC}$ impact on the transcriptome in neurons, we performed whole-transcript RNA-seq on primary neuron cultures transfected with either 5'tiRNA$^{Gly\text{-}GCC}$ mimic or scrambled control. RNA-seq generated between 25 million and 60 million reads per sample (Supplementary Fig. S3a), and the genome mapping rate was around 80 % for each sample (Supplementary Fig. S3b), indicative of high-quality samples (Conesa et al., 2016). Prior to sequencing, the RNA samples underwent poly-A selection to deplete ribosomal RNA (rRNA) and enrich for mRNA. However, other RNA species with poly-A tails, such as long non-coding RNAs (lncRNAs), were also captured using whole-transcript RNA-seq (Supplementary Fig. S3c). Given that tiRNAs may influence different RNA species in distinct ways, differential expression analyses were conducted separately for mRNAs and lncRNAs.

Interestingly, despite successful transfection and sequencing, no significant DE mRNAs or lncRNAs were identified in the 5'tiRNA$^{Gly\text{-}GCC}$-transfected neurons compared to control when corrected for multiple comparisons (adjusted *p*-value <0.05; Supplementary Table S1). As this was an exploratory study, we next used a less stringent *p*-value threshold (unadjusted *p*-value <0.05) to select a set of preliminary DE mRNA and lncRNA for downstream analysis to identify potential cellular processes affected by 5'tiRNA$^{Gly\text{-}GCC}$. A total of 604 DE mRNAs were identified (569 downregulated, 35 upregulated), along with 39 DE lncRNAs (34 downregulated, 5 upregulated), in response to 5'tiRNA$^{Gly\text{-}GCC}$ (Fig. 3a-b, Supplementary Table S1). Next, we used RNA-hybrid to identify any potential 5'tiRNA$^{Gly\text{-}GCC}$-binding sites on the DE mRNAs and lncRNAs identified by RNA-seq. The RNAhybrid analysis revealed that 335 DE mRNAs and 25 DE lncRNAs contained predicted 5'tiRNA$^{Gly\text{-}GCC}$ binding sites (Fig. 3c and Supplementary Table S2 for mRNAs, Fig. 3d and Supplementary Table S3 for lncRNAs), suggesting that these transcripts

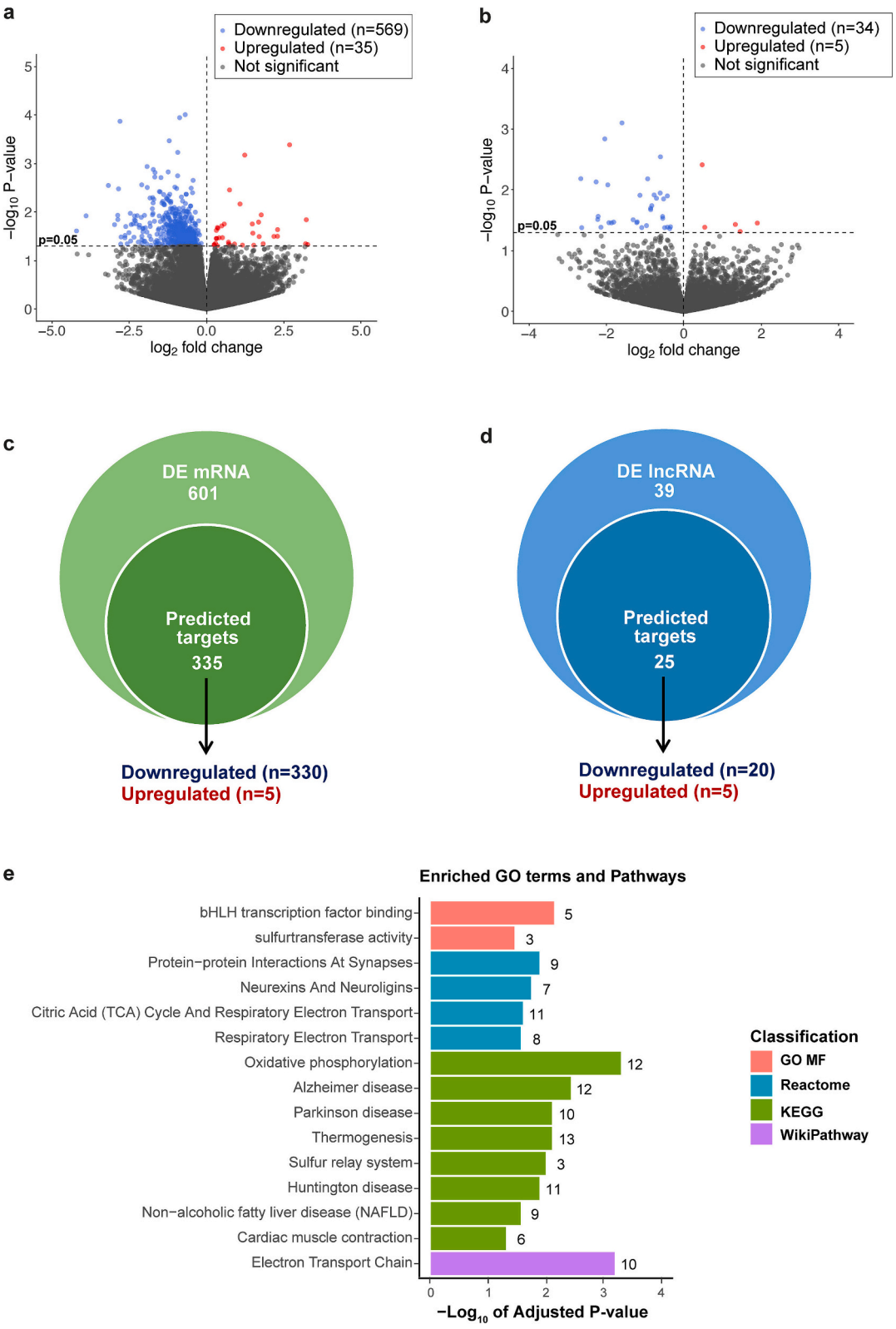

Fig. 3. Analysis of RNA-seq data. A-B Volcano plot of differentially expressed (DE, *p*-value <0.05) A mRNAs and B lncRNAs in 5'tiRNA$^{Gly\text{-}GCC}$–transfected neurons ($n = 5$) versus scrambled control ($n = 5$). Grey dots indicate not significantly regulated genes. Horizontal dashed line indicates *p*-value<0.05 and vertical dashed line indicates $\log_2$ fold change = 0. C Stacked Venn diagram depicting the number of DE mRNA containing 5'tiRNA$^{Gly\text{-}GCC}$ binding site(s) (RNA-hybrid predicted targets of 5'tiRNA$^{Gly\text{-}GCC}$) D Stacked Venn diagram depicting the number of DE lncRNA containing 5'tiRNA$^{Gly\text{-}GCC}$ binding site(s) (RNA-hybrid predicted targets of 5'tiRNA$^{Gly\text{-}GCC}$). E Enriched GO Molecular Function (MF) terms and pathways from each pathway database (Reactome, KEGG and WikiPathways) for the downregulated DE mRNAs containing 5'tiRNA$^{Gly\text{-}GCC}$ binding sites (adjusted *p*-value <0.05). Colours represent GO or pathway database: GO (red), Reactome (blue), KEGG (green), and WikiPathway (purple). Number next to bar = gene count. (For interpretation of the references to colour in this figure legend, the reader is referred to the web version of this article.)

Table 1
Top 10 differentially expressed mRNA and lncRNA (p-value <0.05 and |log2FC| > 1) with potential 5'tiRNA$^{Gly\text{-}GCC}$ binding sites, identified in the 5'tiRNA$^{Gly\text{-}GCC}$-transfected neurons compared to scrambled control. Genes are ranked based on p-value.

Gene type	Gene name	log2FC	p-value
mRNA	*Gng13*	−2.80	1.35E-04
	Ppp1r35	−1.92	1.16E-03
	Cort	−1.24	1.50E-03
	Cartpt	−1.02	3.07E-03
	Bola1	−1.52	3.80E-03
	Nr2f6	−1.50	3.86E-03
	Rell2	−1.19	4.31E-03
	Abhd8	−1.23	4.73E-03
	Cox11	−1.70	5.49E-03
	Vgf	−1.24	5.70E-03
lncRNA	*4921529L05Rik*	1.90	3.50E-02
	Gm45353	1.46	4.82E-02
	Gm44686	1.33	3.69E-02
	Gm15860	−1.09	4.16E-02
	2310010J17Rik	−1.13	1.22E-02
	Gm7008	−1.20	3.35E-02
	Mtag2	−1.93	3.45E-02
	Gm30025	−2.04	1.45E-03
	2410080I02Rik	−2.14	4.10E-02
	Gm26833	−2.21	2.72E-02

may be directly regulated by 5'tiRNA$^{Gly\text{-}GCC}$ interactions. Interestingly, the regions of complementarity extended beyond a "seed" region of 6–8 bp complementarity which is commonly found between microRNAs (miRNAs) and their target transcripts (Bartel, 2009) (Supplementary Fig. S4), suggesting an alternative method of gene expression regulation may be occurring. Additionally, 330 of the 335 predicted mRNA targets and 20 of the 25 predicted lncRNA targets were downregulated (Fig. 3c-d), indicating that 5'tiRNA$^{Gly\text{-}GCC}$ may function to silence gene expression through complementary binding. The top 10 DE mRNAs and lncRNAs containing predicted 5'tiRNA$^{Gly\text{-}GCC}$ binding sites are found in Table 1. Of note, the majority of the top DE mRNAs listed in Table 1 contain potential 5'tiRNA$^{Gly\text{-}GCC}$ binding sites located within either the 5′ untranslated region (5'UTR) or the coding sequence (CDS), but binding sites in the 3′ untranslated region (3'UTR) also occurred among the DE mRNAs (Supplementary Table S2). Supplementary Fig. S4 shows the top three tiRNA-mRNA and tiRNA-lncRNA interactions that exhibit the lowest mfe for the mRNAs and lncRNAs presented in Table 1. The most significantly DE mRNA and predicted target of 5'tiRNA$^{Gly\text{-}GCC}$ was *Gn13*, encoding G protein Subunit Gamma 13, which is essential for regulating GTPase activity. Among the other top DE mRNAs were several genes encoding neuropeptides, including *Vgf, Cort and Cartpt*. VGF, or VGF nerve growth factor inducible, is a secreted neuroendocrine polypeptide found to be reduced in the CSF of ALS patients (Pasinetti et al., 2006). Both *Cort* and *Cartpt* also encode neuroendocrine peptides that are widely expressed in the CNS and play key roles in regulating the stress response (Bale and Vale, 2004; Rogge et al., 2008). In contrast, the majority of the top DE lncRNAs were Gm genes and riken cDNA genes, which currently lack functional annotations.

To get a better understanding of the functions of the DE mRNAs containing predicted 5'tiRNA$^{Gly\text{-}GCC}$ binding sites, we performed functional enrichment analysis. No significant GO terms or pathways were identified for the upregulated mRNAs, likely due to their small number ($n = 5$). However, analysis of the downregulated DE mRNAs revealed enrichment of pathways related to neurotransmitter release, synapse formation and maintenance (Fig. 3e, Supplementary Table S4). Additionally, several significantly enriched pathways among the downregulated mRNAs were associated with the electron transport chain (ETC), in which dysfunction is linked to oxidative stress and neurodegeneration through the production of reactive oxygen species (Bustamante-Barrientos et al., 2023). The enrichment of multiple pathways related to neurodegenerative diseases further reflects the downregulation of mRNAs involved in the ETC.

3.4. Transfection of 5'tiRNA$^{Gly\text{-}GCC}$ mediates changes at the proteome level in primary neurons

Next, we performed label-free quantitative LC-MS/MS on cultures of mouse primary neurons transfected with synthetic mimics of either 5'tiRNA$^{Gly\text{-}GCC}$ or scrambled tiRNA control. Differential expression analysis identified a total of 212 DE proteins, of which 29 were upregulated and 183 were downregulated, in the 5'tiRNA$^{Gly\text{-}GCC}$-transfected neurons compared to scrambled control (Fig. 4a, Supplementary Table S5). The top 10 identified DE proteins are listed in Table 2. Of note, the top hits were all downregulated in response to 5'tiRNA$^{Gly\text{-}GCC}$, indicating that this 5'tiRNA negatively regulates the proteomic profile of neurons. The most significant downregulated protein was BAG1, a co-chaperone for HSP70 involved in proteostasis, one of the key processes proposed to be dysregulated in ALS and other neurodegenerative diseases (Takayama et al., 1997; Alberti et al., 2003; Webster et al., 2017). Interestingly, elevated levels of BAG1 have been found in the skeletal muscles of SOD1^{G93A} ALS TG mice (Crippa et al., 2013), and the protein has also been reported to mediate neuroprotection in models of Parkinson's disease and Huntington's disease (Sroka et al., 2009; Kermer et al., 2015). Other proteins involved in the regulation of cellular stress responses and proteostasis, such as DNAJB11 and the ubiquitin-activating enzyme UBA3, were also identified as top DE proteins following 5'tiRNA$^{Gly\text{-}GCC}$-transfection (Table 2), indicating that proteins involved in stress responses may be key targets of 5'tiRNA$^{Gly\text{-}GCC}$.

An integrated analysis of the transcriptomic and proteomic data demonstrated that some DE mRNAs/proteins were common across both datasets: *Cep170b, Irf2bpl, Psd, Rplp2, Snrpf* (Supplementary fig. S5a-b). Four of the shared mRNAs/proteins were downregulated at both the transcript and protein levels, while *Irf2bpl* was found downregulated at the mRNA level and upregulated at the protein level (Supplementary fig. S5b). The lack of correlation between gene and protein levels suggests that 5'tiRNA$^{Gly\text{-}GCC}$ regulation may involve distinct mechanisms for different transcripts, resulting in varying effects on mRNA and protein expression levels.

To further investigate potential mechanisms by which 5'tiRNA$^{Gly\text{-}GCC}$ regulates the proteome in neurons, we performed GO term and pathway enrichment analysis of the set of upregulated and downregulated DE proteins, separately. Complete lists of significantly enriched GO terms, KEGG pathways, Reactome pathways and WikiPathways can be found in Supplementary Table S6. Due to the small number of upregulated DE proteins annotated to each GO term and pathway (Supplementary Table S6), we decided to focus on the results obtained for the downregulated DE proteins. Treemap-based hierarchical clustering analysis was performed to identify non-redundant GO biological processes enriched among the downregulated DE proteins. The resulting treemap consisted of six clusters, including 'translation', 'ribonucleoprotein complex assembly', 'Golgi vesicle transport', 'gene expression', 'regulation of mRNA stability' and 'viral process' (Fig. 4b). The major cluster, 'translation', encompassed GO terms associated with protein synthesis and metabolism. The pathway enrichment analysis reflected these results, revealing 'metabolism of proteins' as the most enriched pathway among the downregulated genes (Fig. 4c). Furthermore, many of the enriched pathways were related to translation, particularly translation initiation. Other notable pathways included 'Metabolism of RNA' and 'Cellular Responses to Stress'. These findings indicate that 5'tiRNA$^{Gly\text{-}GCC}$ affects proteins involved in post-transcriptional and translational control of gene expression during conditions of cellular stress. Additionally, we identified enrichment of pathways related to fatty acid beta-oxidation including the metabolic protein ACSL3. This is of particular interest, as our group recently found ACSL3 to be overexpressed in the cerebral cortex of pre-symptomatic TDP-43^{A315T} ALS/FTDTG mice (PND 60) and FUS (1–359) ALS TG mice (PND50), suggesting a role for this protein in early ALS progression (Matveeva et al., 2023).

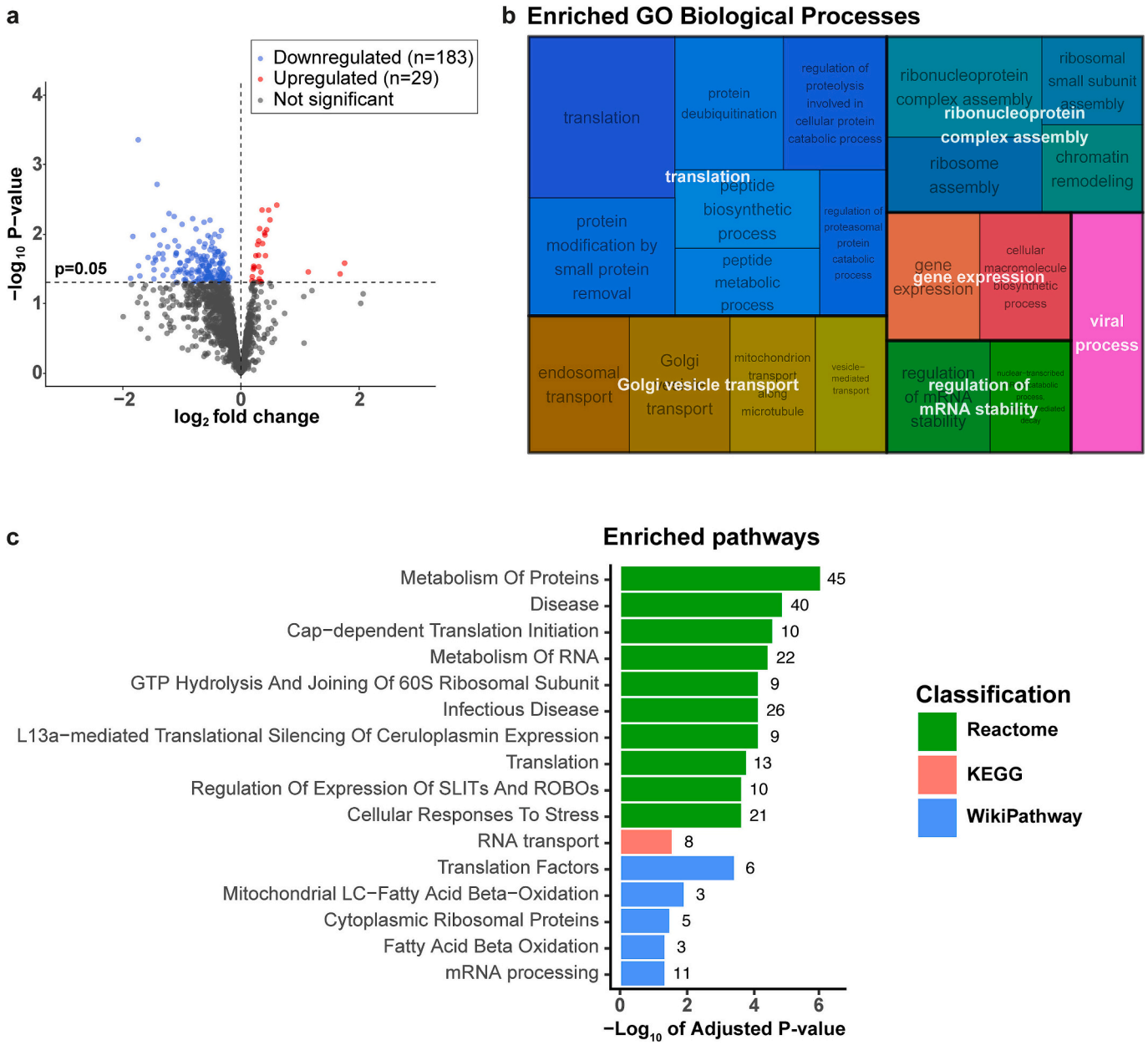

Fig. 4. Differential expression analysis and functional enrichment analysis of proteomics data. A Volcano plot of differentially expressed (DE) proteins (p-value <0.05) in 5'tiRNA$^{Gly\text{-}GCC}$–transfected neurons (n = 5) versus scrambled control (n = 5). Blue and red dots indicate downregulated and upregulated DE proteins, respectively. Grey dots indicate non-significant proteins. Horizontal dashed line indicates p-value <0.05 and vertical dashed line indicates log2 fold change = 0. B Treemap of enriched Gene Ontology (GO) Biological Processes (BP) terms (adjusted p-value <0.05) for the downregulated DE proteins identified in 5'tiRNA$^{Gly\text{-}GCC}$ transfected neurons. Each box in the treemap represents a GO BP, indicated in grey text, and the size of the box is inversely proportional to the enrichment adjusted p-value. Similar terms are grouped (coloured) based on their parent, which is indicated in white text. C Top 10 most enriched pathways from each pathway database (Reactome, KEGG and WikiPathways) for the downregulated DE proteins (adjusted p-value <0.05). Colours represent pathway database: Reactome (green), KEGG (red) and WikiPathway (blue). Number next to bar = protein count. (For interpretation of the references to colour in this figure legend, the reader is referred to the web version of this article.)

3.5. PPI network analysis of the proteome suggests that 5'tiRNA$^{Gly\text{-}GCC}$ regulates proteins linked to ALS and other neurodegenerative diseases

To gain further insight into tiRNA-mediated effects on signaling pathways, we performed PPI network analysis of the complete set of DE proteins identified in the 5'tiRNA$^{Gly\text{-}GCC}$-transfected neurons compared to scrambled control. The resulting PPI network consisted of 212 nodes connected via 232 edges (Fig. 5a). We used the MCODE clustering algorithm to identify densely connected regions in the PPI network and found nine clustered subnetworks. The top 3 significant clusters were selected for further functional pathway analysis (Fig. 5b-d, Supplementary Table S7). The top-scoring cluster included ribosomal proteins that were all annotated to the significantly enriched pathway 'Ribosome' (Fig. 5b). Cluster 2 comprised proteasome subunits and deubiquitinating enzymes associated with the proteasome (Fig. 5c). Interestingly, Cluster 2 also demonstrated enrichment of several pathways of neurodegenerative diseases, including 'Amyotrophic lateral sclerosis', 'Parkinson's disease', 'Alzheimer's disease', 'Huntington's disease', 'Prion disease' and 'Spinocerebellar ataxia' (Fig. 5c), reflecting that proteasomal defects occur in multiple neurodegenerative diseases. This provides further evidence for a role of 5'tiRNAs in neurodegeneration. The interconnected proteins in Cluster 3 are associated

Table 2
Top 10 differentially expressed proteins (p-value <0.05 and |log2FC| > 1) identified in the 5'tiRNA$^{Gly\text{-}GCC}$-transfected neurons versus control, ranked based on p-value.

Protein name	Gene name	log2FC	p-value
BAG family molecular chaperone regulator 1	*Bag1*	−1.74	4.39E-04
Echinoderm microtubule-associated protein-like 4	*Eml4*	−1.42	1.92E-03
NEDD8-activating enzyme E1 catalytic subunit	*Uba3*	−1.21	5.07E-03
Chromobox protein homolog 3	*Cbx3*	−1.13	5.57E-03
DnaJ homolog subfamily B member 11	*Dnajb11*	−1.63	8.73E-03
Centrosomal protein of 170 kDa protein B	*Cep170b*	−1.30	8.75E-03
Complement component 1 Q subcomponent-binding protein, mitochondrial	*C1qbp*	−1.48	1.03E-02
Microtubule-associated protein 1S	*Map1s*	−1.83	1.08E-02
Complexin-1	*Cplx1*	−1.11	1.24E-02
Metastasis-associated protein MTA2	*Mta2*	−1.37	1.44E-02

with the spliceosome (Fig. 5d), a large ribonucleoprotein complex that catalyses pre-mRNA splicing (Lamond, 1993). Of note, defects in the spliceosome machinery are linked to ALS (Tsuiji et al., 2013; La Cognata et al., 2020). These findings, together with our results, further strengthen the link between 5'tiRNA$^{Gly\text{-}GCC}$ and ALS.

To identify the most interconnected proteins in the PPI network, we performed hub gene analysis using the Cytoscape plugin *Cytohubba*. The top 20 hub genes selected based on MCC score are shown in Fig. 6a and also listed in Supplementary Table S8. Among these were genes encoding ribosomal proteins, proteasome subunits, eukaryotic translation initiation factors (eIFs), and deubiquitinating enzymes, many of which were also identified in the PPI clusters. The outcome of the functional enrichment analysis of the hub genes also resonated with the results of the DE protein analysis, identifying GO terms and pathways related to translation, RNA processing and protein metabolism (Fig. 6b, Supplementary Table S9).

4. Discussion

In recent years, dysregulated levels of tiRNAs have been reported in several neurodegenerative and neurological disorders, including ALS (Hogg et al., 2020; Joilin et al., 2020; Magee et al., 2019; Wu et al., 2021; Hogg et al., 2019). Yet, the functional role of tiRNAs in neuronal stress responses during neurodegeneration remains elusive. This is, to the best of our knowledge, the first study to explore the genome-wide effects of tiRNAs on regulation of gene and protein expression in neurons, shedding further light on potential mechanisms by which an ALS-associated tiRNA, 5'tiRNA$^{Gly\text{-}GCC}$, regulates neuronal stress responses in ALS.

Recent work has demonstrated induction of specific 5'tiRNAs, including 5'tiRNA$^{Gly\text{-}GCC}$, in response to arsenite-induced oxidative stress in primary mouse fibroblasts as well as in various cell lines, including HeLa cells, U2OS cells and PC12 neuronal cells (Elkordy et al., 2018; Sanadgol et al., 2022). Here, we report a robust increase in 5'tiRNA$^{Gly\text{-}GCC}$ production also in primary neurons following arsenite-induced oxidative stress. Furthermore, we also demonstrated induction of 5'tiRNA$^{Gly\text{-}GCC}$ in primary neurons in response to epoxomicin-induced proteasomal stress and glutamate-induced excitotoxicity, two other types of stress implicated in ALS (Taylor et al., 2016). It should be noted that a more robust tiRNA production was observed following oxidative stress compared to proteasomal stress and excitotoxic stress, which further underscores oxidative stress as a key mediator of ANG-induced tRNA cleavage. In addition to our findings in vitro, we identified increased expression of 5'tiRNA$^{Gly\text{-}GCC}$ in the lumbar spinal cord of the TDP-43^{A315T} TG mouse model of ALS and FTD, both at the pre-symptomatic stage and at symptom onset. Slightly elevated levels of 5'tiRNA$^{Gly\text{-}GCC}$ were also observed in the spinal cord of FUS (1–359) TG mice and SOD1^{G93A} TG mice at early stages of disease, which adds to previous work from our group where another 5'tiRNA, 5'tiRNA$^{Val\text{-}CAC}$, was found upregulated at symptom onset in the spinal cord of these two animal models (Hogg et al., 2020). Collectively, our findings highlight a role for 5'tiRNA$^{Gly\text{-}GCC}$ production during neuronal stress conditions in ALS.

To investigate the impact of 5'tiRNA$^{Gly\text{-}GCC}$ on neuronal transcriptomic and proteomic profiles, we performed whole-transcript RNA-seq and label-free proteomics on primary neurons transfected with a synthetic mimic of this tiRNA. Notably, approximately half of the dysregulated mRNA transcripts following tiRNA-transfection contained predicted binding sites for 5'tiRNA$^{Gly\text{-}GCC}$, suggesting they may be direct targets of this tiRNA. A similar observation was made for the dysregulated lncRNAs, many of which contained predicted 5'tiRNA$^{Gly\text{-}GCC}$ binding sites. Moreover, the majority of DE transcripts were downregulated, indicating that 5'tiRNA$^{Gly\text{-}GCC}$ may function to silence target mRNAs through complementary base-pairing. These findings align with previous work by Jehn et al. (Jehn et al., 2020), which suggested that transfection with specific 5'tiRNA mimics, including 5'tiRNA$^{Gly\text{-}GCC}$ and 5'tiRNA$^{Glu\text{-}CTC}$, reduces gene expression in HEK293 cells via complementary binding to mRNAs, resulting in decreased transcript levels. However, while their study proposed that 5'tiRNA$^{Gly\text{-}GCC}$ and 5'tiRNA$^{Glu\text{-}CTC}$ silence gene expression by binding their mid-region sequences to the 3'UTR or the CDS of target mRNAs, the majority of the top DE mRNAs in our study all contained 5'tiRNA$^{Gly\text{-}GCC}$ binding sites in either the CDS or 5'UTR. Jehn et al. (Jehn et al., 2020) also found that 5'tiRNA$^{Glu\text{-}CTC}$, but not 5'tiRNA$^{Gly\text{-}GCC}$, could stabilize some mRNAs, an effect we did not observe at either the transcript level or protein level, as discussed further below. The downregulated DE mRNAs predicted to be direct targets of 5'tiRNA$^{Gly\text{-}GCC}$ were associated with pathways involved in energy metabolism and synaptic function, both of which are critical in the pathogenesis of ALS. However, it is essential to further validate these potential tiRNA targets and their biological significance in vitro. Collectively, the findings of this study suggest that 5'tiRNA$^{Gly\text{-}GCC}$ fine-tunes the neuronal transcriptome by selectively modulating specific RNA transcripts as part of a neuronal stress response. Future work should focus on mapping the full repertoire of RNAs, including other sncRNAs, that may be regulated by this and other tiRNAs.

Consistent with our transcriptomics study, the proteomics analysis revealed that the majority of DE proteins in response to 5'tiRNA$^{Gly\text{-}GCC}$ transfection were downregulated, indicating that this tiRNA negatively regulates protein expression. The limited correlation between downregulated transcripts and proteins in our data suggests that 5'tiRNA$^{Gly\text{-}GCC}$ may affect gene expression and protein production through different mechanisms. In particular, we found that transfecting primary neurons with 5'tiRNA$^{Gly\text{-}GCC}$ resulted in downregulation of proteins involved in protein synthesis. More specifically, hub genes encoding eIFs and ribosomal proteins were downregulated, along with an enrichment of biological processes and pathways related to cap-dependent translation initiation, the major rate-limiting step for protein synthesis under physiological conditions and the primary target of translational control during cellular stress (Holcik and Sonenberg, 2005; Hershey et al., 2007). This broad downregulation of proteins within the protein translation machinery, in contrast to the more targeted changes on the transcript level, may reflect a generalised inhibition of translation by 5'tiRNA$^{Gly\text{-}GCC}$, as has been previously proposed for 5'tiRNAs (Yamasaki et al., 2009; Ivanov et al., 2011; Emara et al., 2010; Goncalves et al., 2016). Importantly, these results support previous studies demonstrating that transfection of another synthetic tiRNA, 5'tiRNA$^{Ala\text{-}AGC}$, inhibits cap-dependent translation by interfering with the assembly of

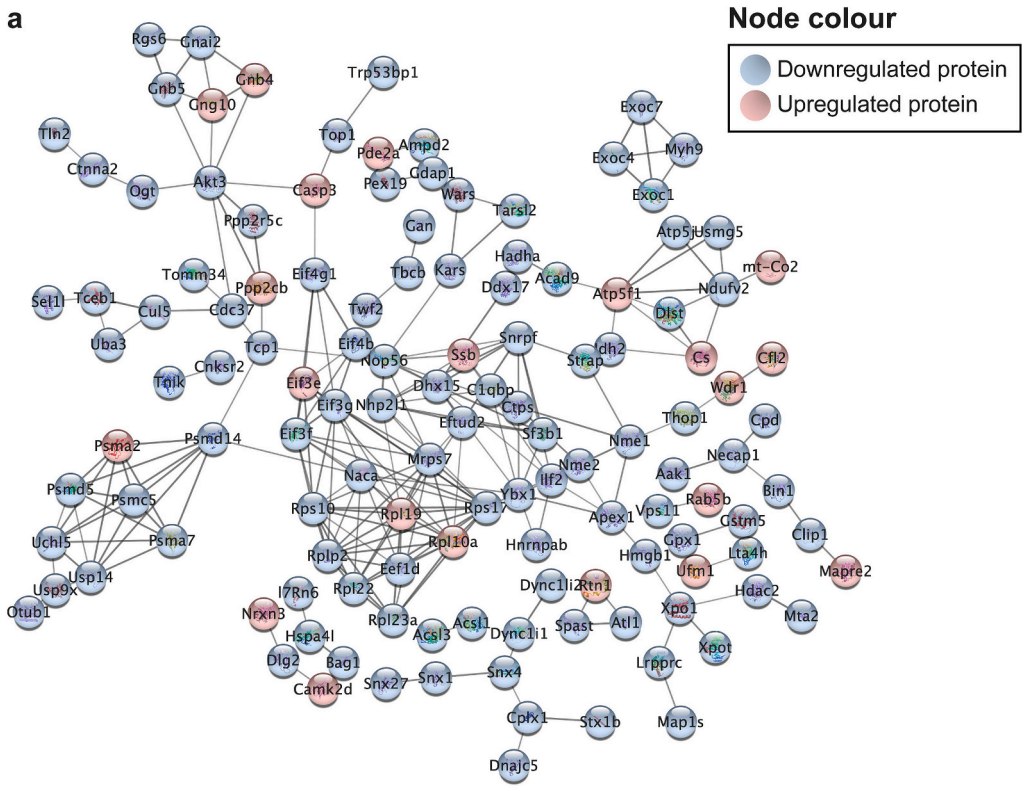

(caption on next page)

Fig. 5. PPI network analysis of proteomics data. A STRING PPI network of differentially expressed proteins (p-value <0.05) identified in the 5'tiRNA$^{Gly\text{-}GCC}$ mimic transfected neurons versus scrambled control (p-value = 3.4e-8). Disconnected nodes are hidden in the PPI network. The node colours indicate protein upregulation (pink) and downregulation (blue). The nodes are labelled with the corresponding gene symbols. B,C,D Top 3 significant clusters identified in A using the MCODE plugin of Cytoscape B MCODE cluster 1 - Ribosome (8 nodes, 28 edges; p-value = 1.0e-16). C MCODE cluster 2 - Neurological disorders (7 nodes, 21 edges; p-value = 1.0e-16). D MCODE cluster 3 - Spliceosome (7 nodes, 14 edges; p-value = 1.5e-12). KEGG pathway enrichment analysis using STRING was applied to each MCODE cluster and nodes annotated to significantly enriched KEGG pathways (adjusted p-value <0.05) are highlighted with coloured circular charts. Enriched KEGG pathways are listed in the figure chart and in Supplementary Table S7. (For interpretation of the references to colour in this figure legend, the reader is referred to the web version of this article.)

the eIF4F complex onto the m7GTP cap structure of mRNA, thereby inhibiting the scanning step of translation initiation (Ivanov et al., 2011; Lyons et al., 2020). In an earlier study, the same group found that 5'tiRNA$^{Ala\text{-}AGC}$ transfection induce SG formation in U2OS cells, albeit at low levels (Emara et al., 2010). In contrast, our results demonstrated no evidence of increased SG formation in neurons following 5'tiRNA$^{Gly\text{-}GCC}$ transfection alone. This observation is consistent with more recent work by Sanadgol et al. (Sanadgol et al., 2022), which reported that specific tiRNAs, including 5'tiRNA$^{Gly\text{-}GCC}$, do not induce SG formation. Additionally, our identification of protein clusters and hub genes associated with ribosome biogenesis are also in line with a previous study where an ANG-induced tiRNA derived from the 3'end of mature tRNA^{Thr} was found to associate with ribosomes and influence protein translation during stress recovery in *Trypanosoma brucei* (Fricker et al., *2019*). While our proteomics analysis point to a role for 5'tiRNA$^{Gly\text{-}GCC}$ in regulation of translation under neuronal stress conditions, future efforts will be aimed at assessing 5'tiRNA$^{Gly\text{-}GCC}$ direct effects on global translation in functional assays, such as in vitro translation reporter assays. Further functional studies are also required to validate potential tiRNA-protein interactions and to determine the mechanisms by which this, and other 5'tiRNAs, may reprogram protein synthesis in neuronal stress responses.

Our studies also suggest a role for 5'tiRNA$^{Gly\text{-}GCC}$ in protein degradation. PPI network analysis of the 5'tiRNA-associated proteome revealed a cluster of proteasome subunits associated with various neurodegenerative diseases, including ALS. The proteasome is a proteolytic enzyme complex responsible for degradation of misfolded or damaged proteins (Bard et al., 2018). Its function is critical for maintaining proteostasis, and dysfunction of the proteasome is implicated in ALS and other neurodegenerative diseases (Medinas et al., 2017). In addition, we also identified enrichment of several biological processes and pathways associated with proteolysis. In conjunction with the observed upregulation of 5'tiRNA$^{Gly\text{-}GCC}$ in neurons in response to proteasomal stress, these findings suggest a potential role for 5'tiRNA$^{Gly\text{-}GCC}$ in regulating proteasome activity, and consequently, protein degradation under neuronal stress responses. However, additional work is required to determine whether 5'tiRNA production is linked to the control of proteostasis in ALS. Moreover, we observed downregulation of proteins associated with fatty acid oxidation following the transfection of primary cortical neurons with 5'tiRNA$^{Gly\text{-}GCC}$. Notably, we previously found one of these proteins, ACSL3, to be upregulated in the cerebral cortex of TDP-43^{A315T} TG mice (PND 60) and FUS (1–359) ALS TG mice (PND 50) (Matveeva et al., 2023). However, levels of 5'tiRNA$^{Gly\text{-}GCC}$ was also found elevated in these animal models in the present study. A possible explanation for this discrepancy is that 5'tiRNA$^{Gly\text{-}GCC}$ may function to modulate stress-induced upregulation of ACSL3 in ALS. Specifically, ACSL3 may be upregulated by other factors, such as the activation of the peroxisome proliferator-activated receptor (PPAR) signaling pathway, as suggested by previous studies (Dervishi et al., 2018). Alternatively, the observed differences could reflect tissue-specific regulatory mechanisms, as ACSL3 was upregulated in the cerebral cortex, whereas tiRNA expression was analyzed in the spinal cord. Therefore, the relationship between 5'tiRNA$^{Gly\text{-}GCC}$ and ACSL3 should be further investigated within the same tissues to better understand their interaction.

Although the results of this study support a role for 5'tiRNA$^{Gly\text{-}GCC}$ in neuronal stress responses and neurodegeneration, there are certain limitations to consider. Research on tiRNAs is still in its infancy and the experimental 'toolbox' to study their biological functions is currently limited. Most studies in the field have employed synthetic tiRNA mimics to investigate the functions of specific tiRNAs (Yamasaki et al., 2009; Ivanov et al., 2014; Ivanov et al., 2011; Emara et al., 2010; Jehn et al., 2020; Goncalves et al., 2016). The physiological levels of intracellular tiRNAs are unknown but believed to be higher than those of other sncRNAs (Li et al., 2022; Mesquita-Ribeiro et al., 2021). Still, introduction of specific tiRNAs through the use of synthetic mimics may lead to higher concentrations of intracellular tiRNAs than occurring in response to stress. For our transfection experiments, we selected the lowest tiRNA mimic concentration (100 nM) that allowed detection by ICC, ensuring intracellular uptake. This concentration is consistent with those used in previous studies, which range from 50 nM to 750 nM (Ivanov et al., 2011; Jehn et al., 2020; Tao et al., 2021). Notably, Ivanov et al. (Ivanov et al., 2011) estimated that stress-induced intracellular levels of two tiRNA species, tiRNA$^{Ala/Cys}$, reach approximately 0.5 μM, with total tiRNA levels in stressed cells amounting to around 5 μM. The concentration of 5'tiRNA$^{Gly\text{-}GCC}$ used in our transfection experiments aligns with these physiological estimates. We achieved robust expression of transfected 5'tiRNA$^{Gly\text{-}GCC}$ in our model system, and still could not detect significant gene expression changes without reducing the stringency of the analysis pipeline. Therefore, we cannot exclude the possibility that the gene expression changes observed are artefacts due to high/non-physiological levels of 5'tiRNA$^{Gly\text{-}GCC}$. However, we can conclude that 5'tiRNA$^{Gly\text{-}GCC}$ does not regulate gene expression in the same manner as miRNAs, where abundant target gene expression changes are detected in response to overexpression of a miRNA mimic. Indeed, the regions of complementarity identified here extend beyond the "seed" regions of binding between miRNAs and their targets, however analysis of Argonaute complexes is required to validate this. Moreover, synthetic tiRNA mimics may lack post-transcriptional modifications and hence may not fully mimic their endogenous equivalents. To overcome the above mentioned caveats of tiRNA "overexpression", an alternative approach would be to silence endogenous tiRNAs using synthetic antisense oligonucleotides (ASOs). This strategy provides added advantageous as ASOs are shorter than tiRNA mimics and can be directly delivered to the culture medium without the need for transfection, which is proven especially difficult in post-mitotic cells such as primary neurons (Sariyer, 2013). However, ASOs directed to tiRNAs may also influence mature tRNA levels as the target sequence is present in both.

In summary, this explorative study provides novel insight into potential mechanisms by which 5'tiRNA$^{Gly\text{-}GCC}$ fine tunes gene expression and protein production in neurons. Our findings further support a role for tiRNAs as part of a protective response against neurodegeneration, underscoring the need for further exploration in ALS.

Funding

This work was supported by funding from the RCSI STAR PhD Programme (to E.J.), from Research Ireland (16/RC/3948, 17/JPND/3455, 20/SP/8953 and 21/RC/10294_P2 co-funded under the European Regional Development Fund and by FutureNeuro and Precision-ALS industry partners) (to J.H.M.P.), and by The Comprehensive Molecular Analytical Platform (CMAP) under the Research Ireland Research Infrastructure Programme, reference 18/RI/5702 (to D.M.). S.B. was supported by Research Ireland CRT in Genomics Data Science under

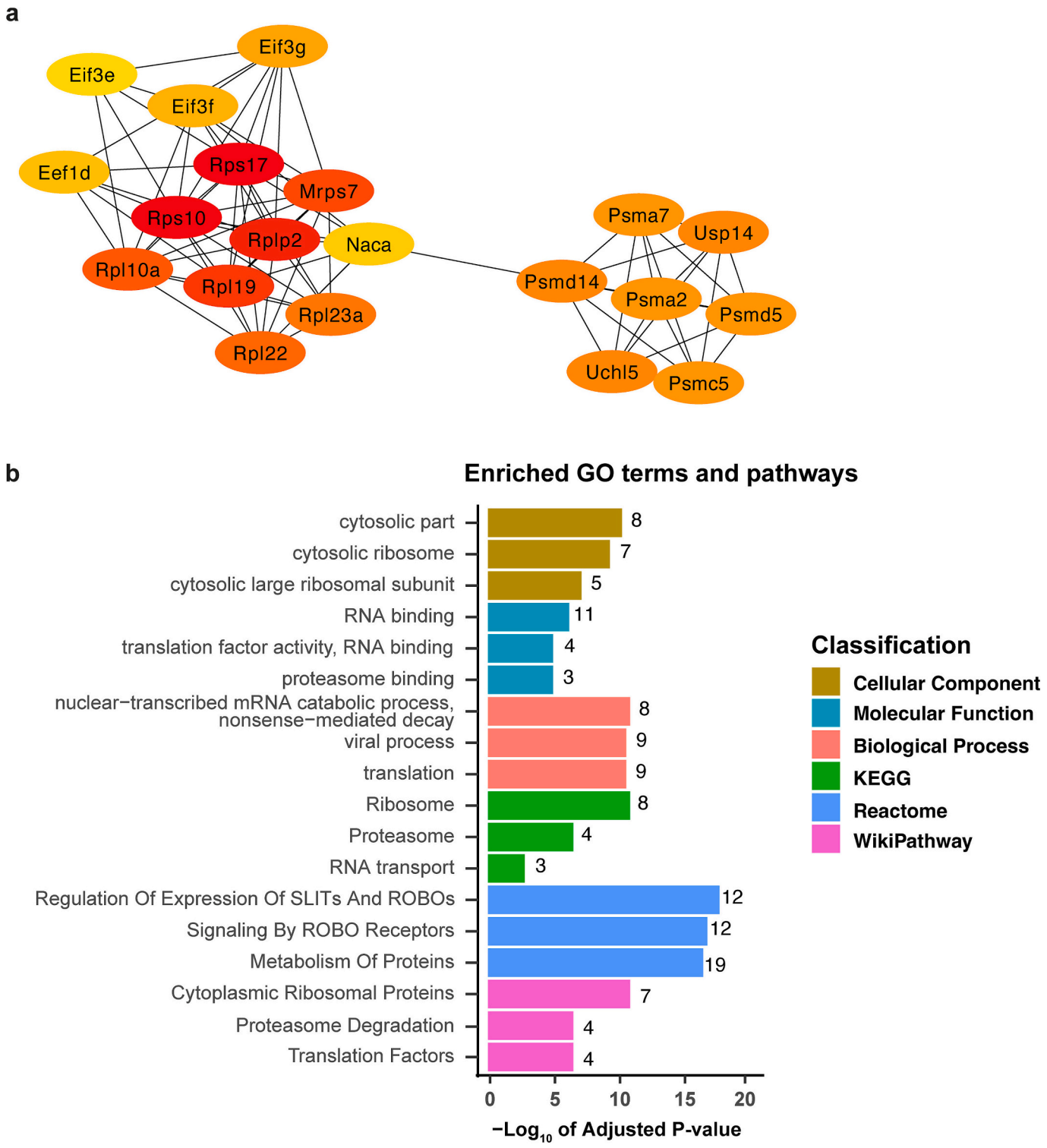

Fig. 6. Hub gene analysis of PPI network. A Top 20 hub genes identified in the PPI network (Fig. 5a) using the Maximal Clique Centrality (MCC) algorithm of the Cytoscape plugin Cytohubba. The node colour denotes interaction degree (red for high degree, orange for intermediate degree, and yellow for low degree). B Top 3 most enriched gene ontology (GO) terms for each GO category (Cellular Component, Molecular Function and Biological Process) and top 3 most enriched pathways from each pathway database (Reactome, KEGG and Wikipathways) identified for the hub genes in the PPI network (cut-off criteria: adjusted *p*-value <0.05). Colours represent GO category or pathway database: Cellular Component (yellow), Molecular Function (cyan), Biological Process (red), KEGG (green), Reactome (blue), WikiPathway (pink). Number next to bar = protein count. (For interpretation of the references to colour in this figure legend, the reader is referred to the web version of this article.)

grant number 18/CRT/6214. Q.M. was funded by the RCSI International StAR Ph.D. scholarship program with Soochow University.

Ethics approval

All animal work was performed in accordance with the European Union Directive (2010/63/EU) with ethical approval by the RCSI Research Ethics Committee (REC1122 and TH007), and under sequential licences from the Health Products Regulatory Authority (AE19127/P004 and AE19127/P054), Dublin, Ireland.

CRediT authorship contribution statement

Elisabeth Jirström: Writing – review & editing, Writing – original draft, Visualization, Validation, Project administration, Methodology, Investigation, Formal analysis, Data curation, Conceptualization. **Anna Matveeva:** Writing – review & editing, Visualization, Investigation, Formal analysis, Data curation. **Sharada Baindoor:** Writing – review & editing, Investigation, Formal analysis, Data curation. **Paul Donovan:** Formal analysis, Data curation. **Qilian Ma:** Writing – review & editing, Investigation, Formal analysis. **Elena Perez Morrissey:** Writing – review & editing, Investigation, Formal analysis. **Ingrid Arijs:** Writing – review & editing, Investigation, Data curation. **Bram Boeckx:** Formal analysis, Data curation. **Diether Lambrechts:** Supervision, Resources. **Amaya Garcia-Munoz:** Investigation, Data curation. **Eugène T. Dillon:** Investigation, Formal analysis, Data curation. **Kieran Wynne:** Writing – review & editing, Data curation. **Zheng Ying:** Writing – review & editing, Supervision. **David Matallanas:** Writing – review & editing, Supervision, Resources, Formal analysis. **Marion C. Hogg:** Writing – review & editing, Methodology, Investigation, Formal analysis, Data curation, Conceptualization. **Jochen H.M. Prehn:** Writing – review & editing, Supervision, Resources, Project administration, Methodology, Funding acquisition, Conceptualization.

Declaration of competing interest

The authors declare that they have no known competing financial interests or personal relationships that could have appeared to influence the work reported in this paper.

Data availability

The RNA-seq raw data have been deposited in ArrayExpress under accession number E-MTAB-13537. The mass spectrometry proteomics data have been deposited to the ProteomeXchange Consortium via the PRIDE partner repository with the dataset identifier PXD046961.

Acknowledgements

We thank Dr. Heiko Düssmann for imaging support and helpful discussions, Ms. Ina Woods for technical assistance, and Dr. Orla Watters, Professor Mark Helm and Professor Jørgen Kjems for technical discussions and advice. The graphical abstract was created in BioRender. fn, b. (2024) https://BioRender.com/i81e847.

Appendix A. Supplementary data

Supplementary data to this article can be found online at https://doi.org/10.1016/j.expneurol.2024.115128.

References

Alberti, S., Esser, C., Höhfeld, J., 2003. BAG-1–a nucleotide exchange factor of Hsc70 with multiple cellular functions. Cell Stress Chaperones 8, 225–231.

Anders, S., Pyl, P.T., Huber, W., 2014. HTSeq—a Python framework to work with high-throughput sequencing data. Bioinformatics 31, 166–169. https://doi.org/10.1093/bioinformatics/btu638.

Ashburner, M., Ball, C.A., Blake, J.A., Botstein, D., Butler, H., Cherry, J.M., Davis, A.P., Dolinski, K., Dwight, S.S., Eppig, J.T., Harris, M.A., Hill, D.P., Issel-Tarver, L., Kasarskis, A., Lewis, S., Matese, J.C., Richardson, J.E., Ringwald, M., Rubin, G.M., Sherlock, G., 2000. Gene ontology: tool for the unification of biology. Nat. Genet. 25, 25–29. https://doi.org/10.1038/75556.

Bader, G.D., Hogue, C.W., 2003. An automated method for finding molecular complexes in large protein interaction networks. BMC Bioinformatics 4, 2. https://doi.org/10.1186/1471-2105-4-2.

Bale, T.L., Vale, W.W., 2004. CRF and CRF receptors: role in stress responsivity and other behaviors. Annu. Rev. Pharmacol. Toxicol. 44, 525–557. https://doi.org/10.1146/annurev.pharmtox.44.101802.121410.

Bard, J.A.M., Goodall, E.A., Greene, E.R., Jonsson, E., Dong, K.C., Martin, A., 2018. Structure and function of the 26S proteasome. Annu. Rev. Biochem. 87, 697–724. https://doi.org/10.1146/annurev-biochem-062917-011931.

Bartel, D.P., 2009. MicroRNAs: target recognition and regulatory functions. Cell 136, 215–233. https://doi.org/10.1016/j.cell.2009.01.002.

Brown, R.H., Al-Chalabi, A., 2017. Amyotrophic lateral sclerosis. N. Engl. J. Med. 377, 162–172. https://doi.org/10.1056/NEJMra1603471.

Burrell, J.R., Kiernan, M.C., Vucic, S., Hodges, J.R., 2011. Motor neuron dysfunction in frontotemporal dementia. Brain 134, 2582–2594. https://doi.org/10.1093/brain/awr195.

Bushnell, B., Rood, J., Singer, E., 2017. BBMerge - accurate paired shotgun read merging via overlap. PLoS One 12, e0185056. https://doi.org/10.1371/journal.pone.0185056.

Bustamante-Barrientos, F.A., Luque-Campos, N., Araya, M.J., Lara-Barba, E., de Solminihac, J., Pradenas, C., Molina, L., Herrera-Luna, Y., Utreras-Mendoza, Y., Elizondo-Vega, R., Vega-Letter, A.M., Luz-Crawford, P., 2023. Mitochondrial dysfunction in neurodegenerative disorders: potential therapeutic application of mitochondrial transfer to central nervous system-residing cells. J. Transl. Med. 21, 613. https://doi.org/10.1186/s12967-023-04493-w.

Chan, P.P., Lowe, T.M., 2009. GtRNAdb: a database of transfer RNA genes detected in genomic sequence. Nucleic Acids Res. 37, D93–D97. https://doi.org/10.1093/nar/gkn787.

Chan, P.P., Lowe, T.M., 2016. GtRNAdb 2.0: an expanded database of transfer RNA genes identified in complete and draft genomes. Nucleic Acids Res. 44, D184–D189. https://doi.org/10.1093/nar/gkv1309.

Chen, E.Y., Tan, C.M., Kou, Y., Duan, Q., Wang, Z., Meirelles, G.V., Clark, N.R., Ma'ayan, A., 2013. Enrichr: interactive and collaborative HTML5 gene list enrichment analysis tool. BMC Bioinformatics 14, 128. https://doi.org/10.1186/1471-2105-14-128.

Chen, Q., Yan, M., Cao, Z., Li, X., Zhang, Y., Shi, J., Feng, G.H., Peng, H., Zhang, X., Zhang, Y., Qian, J., Duan, E., Zhai, Q., Zhou, Q., 2016. Sperm tsRNAs contribute to intergenerational inheritance of an acquired metabolic disorder. Science 351, 397–400. https://doi.org/10.1126/science.aad7977.

Chin, C.H., Chen, S.H., Wu, H.H., Ho, C.W., Ko, M.T., Lin, C.Y., 2014. cytoHubba: identifying hub objects and sub-networks from complex interactome. BMC Syst. Biol. 8, S11. https://doi.org/10.1186/1752-0509-8-S4-S11.

Concannon, C.G., Tuffy, L.P., Weisová, P., Bonner, H.P., Dávila, D., Bonner, C., Devocelle, M.C., Strasser, A., Ward, M.W., Prehn, J.H., 2010. AMP kinase-mediated activation of the BH3-only protein Bim couples energy depletion to stress-induced apoptosis. J. Cell Biol. 189, 83–94. https://doi.org/10.1083/jcb.200909166.

Conesa, A., Madrigal, P., Tarazona, S., Gomez-Cabrero, D., Cervera, A., McPherson, A., Szcześniak, M.W., Gaffney, D.J., Elo, L.L., Zhang, X., Mortazavi, A., 2016. A survey of best practices for RNA-seq data analysis. Genome Biol. 17, 13. https://doi.org/10.1186/s13059-016-0881-8.

Coughlan, K.S., Halang, L., Woods, I., Prehn, J.H., 2016. A high-fat jelly diet restores bioenergetic balance and extends lifespan in the presence of motor dysfunction and lumbar spinal cord motor neuron loss in TDP-43A315T mutant C57BL6/J mice. Dis. Model. Mech. 9, 1029–1037. https://doi.org/10.1242/dmm.024786.

Cox, J., Mann, M., 2008. MaxQuant enables high peptide identification rates, individualized p.p.b.-range mass accuracies and proteome-wide protein quantification. Nat. Biotechnol. 26, 1367–1372. https://doi.org/10.1038/nbt.1511.

Crippa, V., Boncoraglio, A., Galbiati, M., Aggarwal, T., Rusmini, P., Giorgetti, E., Cristofani, R., Carra, S., Pennuto, M., Poletti, A., 2013. Differential autophagy power in the spinal cord and muscle of transgenic ALS mice. Front. Cell. Neurosci. 7, 234. https://doi.org/10.3389/fncel.2013.00234.

Dervishi, I., Gozutok, O., Murnan, K., Gautam, M., Heller, D., Bigio, E., Ozdinler, P.H., 2018. Protein-protein interactions reveal key canonical pathways, upstream regulators, interactome domains, and novel targets in ALS. Sci. Rep. 8, 14732. https://doi.org/10.1038/s41598-018-32902-4.

Dobin, A., Davis, C.A., Schlesinger, F., Drenkow, J., Zaleski, C., Jha, S., Batut, P., Chaisson, M., Gingeras, T.R., 2012. STAR: ultrafast universal RNA-seq aligner. Bioinformatics 29, 15–21. https://doi.org/10.1093/bioinformatics/bts635.

Doncheva, N.T., Morris, J.H., Gorodkin, J., Jensen, L.J., 2019. Cytoscape StringApp: network analysis and visualization of proteomics data. J. Proteome Res. 18, 623–632. https://doi.org/10.1021/acs.jproteome.8b00702.

Elkordy, A., Mishima, E., Niizuma, K., Akiyama, Y., Fujimura, M., Tominaga, T., Abe, T., 2018. Stress-induced tRNA cleavage and tiRNA generation in rat neuronal PC12 cells. J. Neurochem. 146, 560–569. https://doi.org/10.1111/jnc.14321.

Emara, M.M., Ivanov, P., Hickman, T., Dawra, N., Tisdale, S., Kedersha, N., Hu, G.F., Anderson, P., 2010. Angiogenin-induced tRNA-derived stress-induced RNAs promote stress-induced stress granule assembly. J. Biol. Chem. 285, 10959–10968. https://doi.org/10.1074/jbc.M109.077560.

Fricker, R., Brogli, R., Luidalepp, H., Wyss, L., Fasnacht, M., Joss, O., Zywicki, M., Helm, M., Schneider, A., Cristodero, M., Polacek, N., 2019. A tRNA half modulates

translation as stress response in Trypanosoma brucei. Nat. Commun. 10, 118. https://doi.org/10.1038/s41467-018-07949-6.
Fu, H., Feng, J., Liu, Q., Sun, F., Tie, Y., Zhu, J., Xing, R., Sun, Z., Zheng, X., 2009. Stress induces tRNA cleavage by angiogenin in mammalian cells. FEBS Lett. 583, 437–442. https://doi.org/10.1016/j.febslet.2008.12.043.
Gillespie, M., Jassal, B., Stephan, R., Milacic, M., Rothfels, K., Senff-Ribeiro, A., Griss, J., Sevilla, C., Matthews, L., Gong, C., Deng, C., Varusai, T., Ragueneau, E., Haider, Y., May, B., Shamovsky, V., Weiser, J., Brunson, T., Sanati, N., Beckman, L., Shao, X., Fabregat, A., Sidiropoulos, K., Murillo, J., Viteri, G., Cook, J., Shorser, S., Bader, G., Demir, E., Sander, C., Haw, R., Wu, G., Stein, L., Hermjakob, H., D'Eustachio, P., 2022. The reactome pathway knowledgebase 2022. Nucleic Acids Res. 50, D687–d692. https://doi.org/10.1093/nar/gkab1028.
Goncalves, K.A., Silberstein, L., Li, S., Severe, N., Hu, M.G., Yang, H., Scadden, D.T., Hu, G.F., 2016. Angiogenin promotes hematopoietic regeneration by dichotomously regulating quiescence of stem and progenitor cells. Cell 166, 894–906. https://doi.org/10.1016/j.cell.2016.06.042.
Goodarzi, H., Liu, X., Nguyen, H.C., Zhang, S., Fish, L., Tavazoie, S.F., 2015. Endogenous tRNA-derived fragments suppress breast cancer progression via YBX1 displacement. Cell 161, 790–802. https://doi.org/10.1016/j.cell.2015.02.053.
Greenway, M.J., Andersen, P.M., Russ, C., Ennis, S., Cashman, S., Donaghy, C., Patterson, V., Swingler, R., Kieran, D., Prehn, J., Morrison, K.E., Green, A., Acharya, K.R., Brown Jr., R.H., Hardiman, O., 2006. ANG mutations segregate with familial and 'sporadic' amyotrophic lateral sclerosis. Nat. Genet. 38, 411–413. https://doi.org/10.1038/ng1742.
Gurney, M.E., Pu, H., Chiu, A.Y., Dal Canto, M.C., Polchow, C.Y., Alexander, D.D., Caliendo, J., Hentati, A., Kwon, Y.W., Deng, H.X., et al., 1994. Motor neuron degeneration in mice that express a human Cu,Zn superoxide dismutase mutation. Science 264, 1772–1775. https://doi.org/10.1126/science.8209258.
Hershey, J.W., Sonenberg, N., Mathews, M., 2007. Translational Control in Biology and Medicine, vol. 48. CSHL Press.
Hogg, M.C., Halang, L., Woods, I., Coughlan, K.S., Prehn, J.H.M., 2018. Riluzole does not improve lifespan or motor function in three ALS mouse models. Amyotroph. Lateral Scler Frontotemporal Degener 19, 438–445. https://doi.org/10.1080/21678421.2017.1407796.
Hogg, M.C., Raoof, R., El Naggar, H., Monsefi, N., Delanty, N., O'Brien, D.F., Bauer, S., Rosenow, F., Henshall, D.C., Prehn, J.H., 2019. Elevation in plasma tRNA fragments precede seizures in human epilepsy. J. Clin. Invest. 129, 2946–2951. https://doi.org/10.1172/jci126346.
Hogg, M.C., Rayner, M., Susdalzew, S., Monsefi, N., Crivello, M., Woods, I., Resler, A., Blackbourn, L., Fabbrizio, P., Trolese, M.C., Nardo, G., Bendotti, C., van den Berg, L. H., van Es, M.A., Prehn, J.H.M., 2020. 5'ValCAC tRNA fragment generated as part of a protective angiogenin response provides prognostic value in amyotrophic lateral sclerosis. Brain. Communications 2, fcaa138. https://doi.org/10.1093/braincomms/fcaa138.
Holcik, M., Sonenberg, N., 2005. Translational control in stress and apoptosis. Nat. Rev. Mol. Cell Biol. 6, 318–327. https://doi.org/10.1038/nrm1618.
Ivanov, P., Emara, M.M., Villen, J., Gygi, S.P., Anderson, P., 2011. Angiogenin-induced tRNA fragments inhibit translation initiation. Mol. Cell 43, 613–623. https://doi.org/10.1016/j.molcel.2011.06.022.
Ivanov, P., O'Day, E., Emara, M.M., Wagner, G., Lieberman, J., Anderson, P., 2014. G-quadruplex structures contribute to the neuroprotective effects of angiogenin-induced tRNA fragments. Proc. Natl. Acad. Sci. U. S. A. 111, 18201–18206. https://doi.org/10.1073/pnas.1407361111.
Jehn, J., Treml, J., Wulsch, S., Ottum, B., Erb, V., Hewel, C., Kooijmans, R.N., Wester, L., Fast, I., Rosenkranz, D., 2020. 5' tRNA halves are highly expressed in the primate hippocampus and might sequence-specifically regulate gene expression. RNA 26, 694–707. https://doi.org/10.1261/rna.073395.119.
Joilin, G., Gray, E., Thompson, A.G., Bobeva, Y., Talbot, K., Weishaupt, J., Ludolph, A., Malaspina, A., Leigh, P.N., Newbury, S.F., Turner, M.R., Hafezparast, M., 2020. Identification of a potential non-coding RNA biomarker signature for amyotrophic lateral sclerosis. Brain. Communications 2, fcaa053. https://doi.org/10.1093/braincomms/fcaa053.
Kanehisa, M., 2019. Toward understanding the origin and evolution of cellular organisms. Protein Sci. 28, 1947–1951. https://doi.org/10.1002/pro.3715.
Kanehisa, M., Goto, S., 2000. KEGG: Kyoto encyclopedia of genes and genomes. Nucleic Acids Res. 28, 27–30. https://doi.org/10.1093/nar/28.1.27.
Kanehisa, M., Furumichi, M., Sato, Y., Ishiguro-Watanabe, M., Tanabe, M., 2021. KEGG: integrating viruses and cellular organisms. Nucleic Acids Res. 49, D545–d551. https://doi.org/10.1093/nar/gkaa970.
Kermer, P., Köhn, A., Schnieder, M., Lingor, P., Bähr, M., Liman, J., Dohm, C.P., 2015. BAG1 is neuroprotective in in vivo and in vitro models of Parkinson's disease. J. Mol. Neurosci. 55, 587–595. https://doi.org/10.1007/s12031-014-0396-2.
Kieran, D., Sebastia, J., Greenway, M.J., King, M.A., Connaughton, D., Concannon, C.G., Fenner, B., Hardiman, O., Prehn, J.H., 2008. Control of motoneuron survival by angiogenin. J. Neurosci. 28, 14056–14061. https://doi.org/10.1523/jneurosci.3399-08.2008.
Kim, H.K., Xu, J., Chu, K., Park, H., Jang, H., Li, P., Valdmanis, P.N., Zhang, Q.C., Kay, M. A., 2019. A tRNA-derived small RNA regulates ribosomal protein S28 protein levels after translation initiation in humans and mice. Cell Rep. 29. https://doi.org/10.1016/j.celrep.2019.11.062, 3816-3824.e3814.
Krey, J.F., Wilmarth, P.A., Shin, J.-B., Klimek, J., Sherman, N.E., Jeffery, E.D., Choi, D., David, L.L., Barr-Gillespie, P.G., 2014. Accurate label-free protein quantitation with high- and low-resolution mass spectrometers. J. Proteome Res. 13, 1034–1044. https://doi.org/10.1021/pr401017h.
Krey, J.F., Scheffer, D.I., Choi, D., Reddy, A., David, L.L., Corey, D.P., Barr-Gillespie, P.G., 2018. Mass spectrometry quantitation of proteins from small pools of developing auditory and vestibular cells. Sci. Data 5, 180128. https://doi.org/10.1038/sdata.2018.128.
Krüger, J., Rehmsmeier, M., 2006. RNAhybrid: microRNA target prediction easy, fast and flexible. Nucleic Acids Res. 34, W451–W454. https://doi.org/10.1093/nar/gkl243.
Kuleshov, M.V., Jones, M.R., Rouillard, A.D., Fernandez, N.F., Duan, Q., Wang, Z., Koplev, S., Jenkins, S.L., Jagodnik, K.M., Lachmann, A., McDermott, M.G., Monteiro, C.D., Gundersen, G.W., Ma'ayan, A., 2016. Enrichr: a comprehensive gene set enrichment analysis web server 2016 update. Nucleic Acids Res. 44, W90–W97. https://doi.org/10.1093/nar/gkw377.
La Cognata, V., Gentile, G., Aronica, E., Cavallaro, S., 2020. Splicing players are differently expressed in sporadic amyotrophic lateral sclerosis molecular clusters and brain regions. Cells 9, 159. https://doi.org/10.3390/cells9010159.
Lamond, A.I., 1993. The spliceosome. Bioessays 15, 595–603. https://doi.org/10.1002/bies.950150905.
Li, H., Handsaker, B., Wysoker, A., Fennell, T., Ruan, J., Homer, N., Marth, G., Abecasis, G., Durbin, R., Subgroup, G.P.D.P., 2009. The sequence alignment/map format and SAMtools. Bioinformatics 25, 2078–2079. https://doi.org/10.1093/bioinformatics/btp352.
Li, S., Xu, Z., Sheng, J., 2018. tRNA-derived small RNA: a novel regulatory small non-coding RNA. Genes 9, 246. https://doi.org/10.3390/genes9050246.
Li, G., Manning, A.C., Bagi, A., Yang, X., Gokulnath, P., Spanos, M., Howard, J., Chan, P. P., Sweeney, T., Kitchen, R., Li, H., Laurent, B.D., Aranki, S.F., Kontaridis, M.I., Laurent, L.C., Van Keuren-Jensen, K., Muehlschlegel, J., Lowe, T.M., Das, S., 2022. Distinct stress-dependent signatures of cellular and extracellular tRNA-derived small RNAs. Adv. Sci. (Weinh) 9, e2200829. https://doi.org/10.1002/advs.202200829.
Livak, K.J., Schmittgen, T.D., 2001. Analysis of relative gene expression data using real-time quantitative PCR and the 2(-Delta Delta C(T)) method. Methods 25, 402–408. https://doi.org/10.1006/meth.2001.1262.
Lorenz, R., Bernhart, S.H., Höner zu Siederdissen, C., Tafer, H., Flamm, C., Stadler, P.F., Hofacker, I.L., 2011. ViennaRNA Package 2.0. Algorithms Mol. Biol. 6, 26. https://doi.org/10.1186/1748-7188-6-26.
Love, M.I., Huber, W., Anders, S., 2014. Moderated estimation of fold change and dispersion for RNA-seq data with DESeq2. Genome Biol. 15, 550. https://doi.org/10.1186/s13059-014-0550-8.
Lucantoni, F., Salvucci, M., Düssmann, H., Lindner, A.U., Lambrechts, D., Prehn, J.H.M., 2021. BCL(X)L and BCL2 increase the metabolic fitness of breast cancer cells: a single-cell imaging study. Cell Death Differ. 28, 1512–1531. https://doi.org/10.1038/s41418-020-00683-x.
Lyons, S.M., Kharel, P., Akiyama, Y., Ojha, S., Dave, D., Tsvetkov, V., Merrick, W., Ivanov, P., Anderson, P., 2020. eIF4G has intrinsic G-quadruplex binding activity that is required for tiRNA function. Nucleic Acids Res. 48, 6223–6233. https://doi.org/10.1093/nar/gkaa336.
Magee, R., Londin, E., Rigoutsos, I., 2019. TRNA-derived fragments as sex-dependent circulating candidate biomarkers for Parkinson's disease. Parkinsonism Relat. Disord. 65, 203–209. https://doi.org/10.1016/j.parkreldis.2019.05.035.
Martens, M., Ammar, A., Riutta, A., Waagmeester, A., Slenter Denise, N., Hanspers, K., Miller, R.A., Digles, D., Lopes Elisson, N., Ehrhart, F., Dupuis, L.J., Winckers, L.A., Coort Susan, L., Willighagen, E.L., Evelo, C.T., Pico, A.R., Kutmon, M., 2021. WikiPathways: connecting communities. Nucleic Acids Res. 49, D613–D621. https://doi.org/10.1093/nar/gkaa1024.
Matveeva, A., Watters, O., Rukhadze, A., Khemka, N., Gentile, D., Perez, I.F., Llorente-Folch, I., Farrell, C., Lo Cacciato, E., Jackson, J., Piazzesi, A., Wischhof, L., Woods, I., Halang, L., Hogg, M., Muñoz, A.G., Dillon, E.T., Matallanas, D., Arijs, I., Lambrechts, D., Bano, D., Connolly, N.M.C., Prehn, J.H.M., 2023. Integrated analysis of transcriptomic and proteomic alterations in mouse models of ALS/FTD identify early metabolic adaptions with similarities to mitochondrial dysfunction disorders. Amyotroph. Lateral Scler Frontotemporal Degener 1–15. https://doi.org/10.1080/21678421.2023.2261979.
Medinas, D.B., Valenzuela, V., Hetz, C., 2017. Proteostasis disturbance in amyotrophic lateral sclerosis. Hum. Mol. Genet. 26, R91–R104. https://doi.org/10.1093/hmg/ddx274.
Mejzini, R., Flynn, L.L., Pitout, I.L., Fletcher, S., Wilton, S.D., Akkari, P.A., 2019. ALS genetics, mechanisms, and therapeutics: where are we now? Front. Neurosci. 13. https://doi.org/10.3389/fnins.2019.01310.
Mesquita-Ribeiro, R., Fort, R.S., Rathbone, A., Farias, J., Lucci, C., James, V., Sotelo-Silveira, J., Duhagon, M.A., Dajas-Bailador, F., 2021. Distinct small non-coding RNA landscape in the axons and released extracellular vesicles of developing primary cortical neurons and the axoplasm of adult nerves. RNA Biol. 18, 832–855. https://doi.org/10.1080/15476286.2021.2000792.
Pascovici, D., Handler, D.C., Wu, J.X., Haynes, P.A., 2016. Multiple testing corrections in quantitative proteomics: a useful but blunt tool. Proteomics 16, 2448–2453. https://doi.org/10.1002/pmic.201600044.
Pasinetti, G.M., Ungar, L.H., Lange, D.J., Yemul, S., Deng, H., Yuan, X., Brown, R.H., Cudkowicz, M.E., Newhall, K., Peskind, E., Marcus, S., Ho, L., 2006. Identification of potential CSF biomarkers in ALS. Neurology 66, 1218–1222. https://doi.org/10.1212/01.wnl.0000203129.82104.07.
R Core Team, 2013. R: A Language and Environment for Statistical Computing. Available via R Foundation for Statistical Computing. https://www.R-project.org/.
Rappsilber, J., Mann, M., Ishihama, Y., 2007. Protocol for micro-purification, enrichment, pre-fractionation and storage of peptides for proteomics using StageTips. Nat. Protoc. 2, 1896–1906. https://doi.org/10.1038/nprot.2007.261.
Ritchie, M.E., Phipson, B., Wu, D., Hu, Y., Law, C.W., Shi, W., Smyth, G.K., 2015. Limma powers differential expression analyses for RNA-sequencing and microarray studies. Nucleic Acids Res. 43, e47. https://doi.org/10.1093/nar/gkv007.

Rogge, G., Jones, D., Hubert, G.W., Lin, Y., Kuhar, M.J., 2008. CART peptides: regulators of body weight, reward and other functions. Nat. Rev. Neurosci. 9, 747–758. https://doi.org/10.1038/nrn2493.

Saikia, M., Krokowski, D., Guan, B.-J., Ivanov, P., Parisien, M., Hu, G.-f., Anderson, P., Pan, T., Hatzoglou, M., 2012. Genome-wide identification and quantitative analysis of cleaved tRNA fragments induced by cellular stress. J. Biol. Chem. 287, 42708–42725. https://doi.org/10.1074/jbc.M112.371799.

Sanadgol, N., König, L., Drino, A., Jovic, M., Schaefer, M.R., 2022. Experimental paradigms revisited: oxidative stress-induced tRNA fragmentation does not correlate with stress granule formation but is associated with delayed cell death. Nucleic Acids Res. 50, 6919–6937. https://doi.org/10.1093/nar/gkac495.

Sariyer, I.K., 2013. Transfection of neuronal cultures. Methods Mol. Biol. (Clifton, NJ) 1078, 133–139. https://doi.org/10.1007/978-1-62703-640-5_11.

Sayols, S., 2020. rrvgo: a Bioconductor package to reduce and visualize Gene Ontology terms.

Sebastià, J., Kieran, D., Breen, B., King, M.A., Netteland, D.F., Joyce, D., Fitzpatrick, S.F., Taylor, C.T., Prehn, J.H., 2009. Angiogenin protects motoneurons against hypoxic injury. Cell Death Differ. 16, 1238–1247. https://doi.org/10.1038/cdd.2009.52.

Shannon, P., Markiel, A., Ozier, O., Baliga, N.S., Wang, J.T., Ramage, D., Amin, N., Schwikowski, B., Ideker, T., 2003. Cytoscape: a software environment for integrated models of biomolecular interaction networks. Genome Res. 13, 2498–2504. https://doi.org/10.1101/gr.1239303.

Sharma, U., Conine, C.C., Shea, J.M., Boskovic, A., Derr, A.G., Bing, X.Y., Belleannee, C., Kucukural, A., Serra, R.W., Sun, F., Song, L., Carone, B.R., Ricci, E.P., Li, X.Z., Fauquier, L., Moore, M.J., Sullivan, R., Mello, C.C., Garber, M., Rando, O.J., 2016. Biogenesis and function of tRNA fragments during sperm maturation and fertilization in mammals. Science 351, 391–396. https://doi.org/10.1126/science.aad6780.

Shelkovnikova, T.A., Peters, O.M., Deykin, A.V., Connor-Robson, N., Robinson, H., Ustyugov, A.A., Bachurin, S.O., Ermolkevich, T.G., Goldman, I.L., Sadchikova, E.R., Kovrazhkina, E.A., Skvortsova, V.I., Ling, S.C., Da Cruz, S., Parone, P.A., Buchman, V.L., Ninkina, N.N., 2013. Fused in sarcoma (FUS) protein lacking nuclear localization signal (NLS) and major RNA binding motifs triggers proteinopathy and severe motor phenotype in transgenic mice. J. Biol. Chem. 288, 25266–25274. https://doi.org/10.1074/jbc.M113.492017.

Sroka, K., Voigt, A., Deeg, S., Reed, J.C., Schulz, J.B., Bähr, M., Kermer, P., 2009. BAG1 modulates huntingtin toxicity, aggregation, degradation, and subcellular distribution. J. Neurochem. 111, 801–807. https://doi.org/10.1111/j.1471-4159.2009.06363.x.

Subramanian, V., Crabtree, B., Acharya, K.R., 2007. Human angiogenin is a neuroprotective factor and amyotrophic lateral sclerosis associated angiogenin variants affect neurite extension/pathfinding and survival of motor neurons. Hum. Mol. Genet. 17, 130–149. https://doi.org/10.1093/hmg/ddm290.

Szklarczyk, D., Gable, A.L., Lyon, D., Junge, A., Wyder, S., Huerta-Cepas, J., Simonovic, M., Doncheva, N.T., Morris, J.H., Bork, P., Jensen, L.J., Mering, C.V., 2019. STRING v11: protein-protein association networks with increased coverage, supporting functional discovery in genome-wide experimental datasets. Nucleic Acids Res. 47, D607–d613. https://doi.org/10.1093/nar/gky1131.

Takayama, S., Bimston, D.N., Matsuzawa, S., Freeman, B.C., Aime-Sempe, C., Xie, Z., Morimoto, R.I., Reed, J.C., 1997. BAG-1 modulates the chaperone activity of Hsp70/Hsc70. EMBO J. 16, 4887–4896. https://doi.org/10.1093/emboj/16.16.4887.

Tao, E.W., Wang, H.L., Cheng, W.Y., Liu, Q.Q., Chen, Y.X., Gao, Q.Y., 2021. A specific tRNA half, 5'tiRNA-His-GTG, responds to hypoxia via the HIF1α/ANG axis and promotes colorectal cancer progression by regulating LATS2. J. Exp. Clin. Cancer Res. 40, 67. https://doi.org/10.1186/s13046-021-01836-7.

Taylor, J.P., Brown, R.H., Cleveland, D.W., 2016. Decoding ALS: from genes to mechanism. Nature 539, 197–206. https://doi.org/10.1038/nature20413.

Tsuiji, H., Iguchi, Y., Furuya, A., Kataoka, A., Hatsuta, H., Atsuta, N., Tanaka, F., Hashizume, Y., Akatsu, H., Murayama, S., Sobue, G., Yamanaka, K., 2013. Spliceosome integrity is defective in the motor neuron diseases ALS and SMA. EMBO Mol. Med. 5, 221–234. https://doi.org/10.1002/emmm.201202303.

Tyanova, S., Temu, T., Sinitcyn, P., Carlson, A., Hein, M.Y., Geiger, T., Mann, M., Cox, J., 2016. The Perseus computational platform for comprehensive analysis of (prote) omics data. Nat. Methods 13, 731–740. https://doi.org/10.1038/nmeth.3901.

Webster, C.P., Smith, E.F., Shaw, P.J., De Vos, K.J., 2017. Protein homeostasis in amyotrophic lateral sclerosis: therapeutic opportunities? Front. Mol. Neurosci. 10, 123. https://doi.org/10.3389/fnmol.2017.00123.

Wegorzewska, I., Bell, S., Cairns, N.J., Miller, T.M., Baloh, R.H., 2009. TDP-43 mutant transgenic mice develop features of ALS and frontotemporal lobar degeneration. Proc. Natl. Acad. Sci. U. S. A. 106, 18809–18814. https://doi.org/10.1073/pnas.0908767106.

Wiśniewski, J.R., Zougman, A., Nagaraj, N., Mann, M., 2009. Universal sample preparation method for proteome analysis. Nat. Methods 6, 359–362. https://doi.org/10.1038/nmeth.1322.

Wolozin, B., Ivanov, P., 2019. Stress granules and neurodegeneration. Nat. Rev. Neurosci. 20, 649–666. https://doi.org/10.1038/s41583-019-0222-5.

Wu, W., Lee, I., Spratt, H., Fang, X., Bao, X., 2021. tRNA-derived fragments in Alzheimer's disease: implications for new disease biomarkers and neuropathological mechanisms. J. Alzheimers Dis. 79, 793–806. https://doi.org/10.3233/jad-200917.

Yamasaki, S., Ivanov, P., Hu, G.F., Anderson, P., 2009. Angiogenin cleaves tRNA and promotes stress-induced translational repression. J. Cell Biol. 185, 35–42. https://doi.org/10.1083/jcb.200811106.